Selenocysteine tRNA methylation promotes oxidative stress resistance in melanoma metastasis

Leona A. Nease[1,2], Kellsey P. Church[1], Ines Delclaux[1], Shino Murakami[2], Maider Astorkia[3], Marwa Zerhouni[1], Graciela Cascio[1], Riley O. Hughes[1,2], Kelsey N. Aguirre[1], Paul Zumbo[3], Lukas E. Dow[1,4,5], Samie Jaffrey[2], Doron Betel[3,6,7], and Elena Piskounova[1,4,8*]

[1]Sandra and Edward Meyer Cancer Center, Weill Cornell Medicine, New York, NY; [2] Department of Pharmacology, Weill Cornell Medicine, New York, NY, [3]Applied Bioinformatics Core, Weill Cornell Medicine, New York, NY 10065, USA, [4]Department of Biochemistry, Weill Cornell Medicine, New York NY, [5]Department of Medicine, Weill Cornell Medicine, New York NY, [6]Institute for Computational Biomedicine, Weill Cornell Medicine, New York, NY, [7]Division of Hematology and Oncology, Department of Medicine, Weill Cornell Medicine, New York, NY 10065, USA, [8]Department of Dermatology, Weill Cornell Medicine, New York, NY, *Corresponding author: Elena Piskounova, PhD, elp2025@med.cornell.edu

Abstract

Selenocysteine-containing proteins play a central role in redox homeostasis. Their translation is a highly regulated process, dependent upon two tRNA^{Sec} isodecoders differing by a single 2'-O-ribose methylation, called Um34. We characterized FTSJ1 as the Um34 methyltransferase and show that its activity is required for efficient selenocysteine insertion at the UGA stop codon during translation. Specifically, Loss of Um34 leads to ribosomal stalling and decreased UGA recoding. FTSJ1-deficient cells are more sensitive to oxidative stress and have decreased metastatic colonization in xenograft models of melanoma metastasis. We found that FTSJ1 mediates efficient translation of selenoproteins essential for the cellular antioxidant response. Our findings uncover a role for tRNA^{Sec} Um34 modification in oxidative stress resistance and highlight FTSJ1 as a potential therapeutic target specific for metastatic disease.

Introduction

tRNA modifications coordinate dynamic changes in protein translation, enabling rapid adaptation and survival under

28 various stress conditions[1, 2]. Modifications on the tRNA anticodon loop specifically affect translational efficiency and
29 fidelity[3, 4]. Selenocysteine-containing proteins maintain redox and ER homeostasis and their translation is regulated by a
30 single methyl group at the wobble position (U_{34}) of the Sec tRNA[5]. Selenocysteine (Sec), the 21st amino acid, is coded for
31 by the UGA stop codon and synthesis of these proteins is energetically costly. Biosynthesis of Sec occurs on its tRNA
32 rather than as a small molecule, and co-translational incorporation of Sec requires a short hairpin structure in the 3' UTR.
33 This Selenocysteine Incorporation Sequence (SECIS) is bound by a complex of proteins containing a Sec-specific
34 elongation factor (EEFSEC), SECIS binding protein 2 (SECISBP2) and SECp43 which position the Sec tRNA for loading onto
35 the ribosome and enable readthrough of the UGA codon.[6-9] (Figure 1A).
36
37 Sec tRNA is hypomodified at only 4 positions - pseudoU55 and m^1A58 are involved in proper folding, while anticodon loop
38 modifications, i^6A37 and mcm^5Um34 (Um34), regulate selenoprotein translation[10]. Sec tRNA exists in two forms: with
39 either the precursor mcm^5U, catalyzed by ALKBH8[11, 12], or with additional 2'O-ribose methylation generating mcm^5Um.
40 Um34 is unique to the Sec tRNA and the final step in its maturation, affecting the tertiary structure of the tRNA.
41 Additionally, Um34 is highly responsive to selenium availability, and has been proposed to increase efficiency of Sec
42 insertion[13, 14]. Previous work has suggested these two isodecoders enable the translation of a hierarchy of Sec-containing
43 proteins[15]. This ensures that only essential selenoproteins are synthesized when selenium is limiting, or conversely, non-
44 essential or stress-related selenoproteins are translated when Um34 is increased.
45
46 There are 25 known selenoproteins, with 11 involved in the cellular antioxidant response. Glutathione peroxidases (GPX1-
47 4, GPX6) detoxify ROS, with GPX4 specifically inhibiting ferroptosis[16-18]. Thioredoxin reductases (TXNRD1-3) reduce
48 oxidized cysteine residues and MSRB1 reduces oxidized methionine[19, 20,21]. SELENOH is a nuclear oxidoreductase that
49 regulates p53 in response to ROS[22], and SELENOO is a mitochondrial AMPylase necessary for cellular oxidative stress
50 response[23]. Other selenoproteins maintain ER homeostasis (SELENOF, K, M, N, S and T), regulating and aiding in protein
51 folding[24]. Enzymes DIO1-3 metabolize thyroid hormone[25] and SELENOP distributes selenium throughout the body[26]. Due
52 to the low pKa of Sec, these enzymes are highly reactive and resist permanent oxidative damage[27, 28].
53
54 We have investigated Um34 function in the context of oxidative stress, given the central role for selenoproteins in

55 oxidative stress resistance. We found Um34 increases with oxidative stress, correlating with increased selenoprotein
56 translation and readthrough of UGA. We characterized FTSJ1 as the Um34 methyltransferase, identifying it as a
57 component of the selenocysteine translation machinery and required for efficient Sec insertion. We found its loss affects
58 translation of antioxidant selenoproteins and sensitizes melanoma cells to oxidative stress. A defining feature of
59 metastasizing cancer cells are high levels of oxidative stress and increased dependence on antioxidant pathways[29]. Our
60 data show that loss of FTSJ1 in melanoma cells has no impact on primary tumor growth but decreases metastatic
61 colonization in distant organs. Our work identifies oxidative stress as a specific context for Um34-mediated selenoprotein
62 translation and highlights FTSJ1 as a potential therapeutic target specific to metastatic disease.
63
64 **RESULTS**
65 *Selenoprotein translation and Um34 increase under oxidative stress*
66 Um34 levels were measured by isolating Sec tRNA using a biotinylated oligo probe coupled with LC-MS/MS analysis
67 (Figure 1B and Extended Figure 1A). To establish the effect of extracellular selenium in melanoma cells, A375 cells were
68 depleted of selenium in serum-free DMEM/F12 media. Um34 levels increased with increasing extracellular selenium, while
69 mcm^5U precursor decreased, showing that selenium regulates Um34 biosynthesis and shifts the ratio between the two
70 Sec tRNA isodecoders in melanoma cells (Figure 1C). Selenoproteins GPX1, GPX4, MSRB1, SELENO H, SELENO K and
71 SELENO S increased under selenium supplementation, while TXNRD1, SEPHS2, SELENO P, N, M and O and did not
72 (Extended Figure 1B). Corresponding mRNA levels did not consistently increase with selenium suggesting this effect is
73 mediated through translation (Extended Figure 1C).
74
75 H_2O_2 treatment increases Um34 modification in MEFs[30] and translation of a subset of antioxidant selenoproteins in
76 HEK293T cells[31]. To establish whether oxidative stress has a similar effect in cancer cells, we treated A375 melanoma cells
77 with H_2O_2 or a global prooxidant, pyocyanin, which increases intracellular levels of H_2O_2 and superoxide[32], a species of
78 ROS produced by mitochondria complex I and III and released by tumor-infiltrating macrophages and neutrophils[33]. Both
79 H_2O_2 and pyocyanin treatment increased Um34 levels. In fact, pyocyanin without selenium increased Um34 to similar
80 levels as selenium supplementation alone (Figure 1D), indicating that oxidative stress drives Um34 biosynthesis
81 independent of selenium status. Oxidative stress increased redox-related selenoproteins (GPX1, GPX4, MSRB1, TXNRD1)

82 in melanoma cell lines (Figure 1E and F) without significant effect on mRNA levels (Figure 1G). Several selenoproteins
83 (SELENOK, SELENOF and SELENOP) were upregulated at the mRNA level suggesting there may be additional
84 transcriptional regulation in response to oxidative stress. Components of the selenocysteine machinery such as SECISBP2
85 and SEPSECS were not affected by either selenium or oxidative stress.
86
87 To measure UGA recoding as a selenocysteine, we established a GFP-Reporter Of Selenocysteine Insertion (gROSI), in
88 which a cysteine71 in the GFP was replaced with a UGA coupled with the 3'UTR GPX4 Selenocysteine Insertion Sequence
89 (SECIS) required for UGA readthrough as a selenocysteine[34] (Figure 1H). Fluorescence of GFP is dependent upon Sec-
90 insertion at the UGA, which was seen with extracellular selenium (Figure 1I). More importantly, gROSI with either GPX1
91 or GPX4 3' UTR SECIS was responsive to oxidative stress induction in the absence of selenium (Figure 1J). The combination
92 of selenium and oxidative stress had an additive effect on Sec-insertion, indicating that Um34 may coordinate selenium
93 and oxidation status to increase selenoprotein translation.
94
95 *FTSJ1 is the Um34 selenocysteine-tRNA methyltransferase*
96 To identify the Um34 methyltransferase, we identified proteins interacting with selenocysteine-specific elongation factor
97 EEFSEC in A375 melanoma cells by proteomics. Out of 15 RNA-modifying enzymes interacting with EEFSEC, FTSJ1 was the
98 only wobble 2'O-ribose-modifying tRNA methyltransferase (Figure 2A and Supplementary Table 2)[35, 36]. We validated
99 FTSJ1 interaction with selenocysteine translation machinery by co-immunoprecipitation of FLAG-tagged FTSJ1 with HA-
100 tagged EEFSEC and SECp43 from A375 melanoma cells (Figure 2B, Extended Figure 2A).
101
102 To determine FTSJ1 binding to $tRNA^{Sec}$, we performed RNA-immunoprecipitation from A375 melanoma cells, using either
103 wildtype or catalytically dead A26P mutant of FTSJ1 (found in patients with X-linked intellectual disability) or known
104 $tRNA^{Sec}$-interacting proteins, ALKBH8 and EEFSEC as positive controls (Figure 2C). We saw significant enrichment in the
105 binding of wildtype FTSJ1 to $tRNA^{Sec}$, which was not observed in mutant A26P (Figure 2D). WDR6, the RNA-adapting
106 partner of FTJS1 also showed enrichment for $tRNA^{Sec}$ binding (Figure 2E). FTSJ1 did bind its known substrate $tRNA^{Phe(GAA)}$
107 but did not show enrichment in binding to other tRNAs such as $tRNA^{Lys(UUU)}$ and $tRNA^{Glu(CUC)}$ (Extended Figure 2B and C).
108

109 To functionally validate FTSJ1, we knocked out *FTSJ1* (*FTSJ1*-KO) in A375 (Figure 2F), SK-MEL28 and SK-MEL2 melanoma
110 cell lines. LC/MS-MS analysis of $tRNA^{Sec}$ showed near-complete loss of Um34 on $tRNA^{Sec}$ in the knockout cells compared
111 to control (Figure 2G and Extended Figure 2D and E). Overexpression of wildtype FTJS1 increased Um34 levels, while
112 catalytically inactive mutant A26P had a dominant negative effect, causing a decrease in Um34 levels (Figure 2H and I and
113 Extended Figure 2F). Overexpression of wildtype FTSJ1 in the knockout cell lines rescued the loss of Um34 levels while
114 mutant A26P had no effect (Extended Figure 2G and H). Finally, extracellular selenium had no effect on Um34 levels in
115 the absence of FTSJ1 demonstrating that FTSJ1 activity is the limiting step of Um34 synthesis (Figure 2J). In fact, there
116 was a marked increase in mcm^5U levels, suggesting a compensatory mechanism by ALKBH8 which generates the mcm^5U
117 precursor. To definitively show FTSJ1 is the $tRNA^{Sec}$ Um34 methyltransferase, we performed an *in vitro* methyltransferase
118 assay with FTSJ1 and WDR6 on $tRNA^{Sec}$ from *FTSJ1*-KO cells. Um34 levels were only detectable in the presence of both
119 FTSJ1 and WDR6 (Figure 2K and Extended Figure 2I and J). These data directly establish FTSJ1 as the Um34
120 methyltransferase, demonstrating that FTSJ1 activity is necessary and sufficient for $tRNA^{Sec}$ Um34 modification.
121
122 *Um34 loss affects translation of a subset of selenoproteins*
123 To systematically assess changes in protein translation in *FTSJ1*-KO cells, we used ribosomal profiling to quantify
124 ribosome-protected fragments (RPFs) across the transcriptome. The density of RPFs positioned at specific codons
125 indicates the average ribosomal dwelling time and reflects the relative ribosome translation speed across each codon[37,
126 38]. Given that FTSJ1 is known to modify other tRNAs (Phe $tRNA^{GAA}$ and Trp $tRNA^{CCA}$) in addition to Sec tRNA, we
127 investigated whether loss of FTSJ1 affects translation of individual codons. We compared ribosomal P-site occupancy in
128 *FTSJ1*-KO and Control A375 melanoma cells in the presence of selenium (30nM) and saw that there was no significant
129 difference in codon usage across the global transcriptome especially for codons coding for Phe(GAA) and Trp(CCA)
130 (Extended Figure 3A). This confirms that while FTSJ1 may lead to loss of modifications on other tRNAs, this does not lead
131 to global defects in translation in melanoma cells.
132
133 If $tRNA^{Sec}$ levels are low and/or the ability to decode UGA is impaired (for instance in *FTSJ1*-KO cells), then ribosomes will
134 accumulate upstream of the UGA and translation will terminate with depletion of ribosomes downstream of the UGA.
135 UGA recoding efficiency is defined by the ratio of RPF 3' to 5' of the Sec UGA. Comparing UGA recoding efficiency in WT

136 A375 melanoma cells in the presence (30nM NaSe) vs absence of selenium, we saw a significant decrease in recoding
137 efficiency when selenium was depleted (Figure 3A). When UGA recoding efficiency was measured in WT vs *FTSJ1*-KO A375
138 melanoma cells in the presence of selenium (30nM NaSe), we saw the same decrease in UGA recoding efficiency in *FTJS1*-
139 KO cells (Figure 3B). As a control we compared *FTSJ1*-KO cells in the presence and absence of selenium (Figure 3C), and
140 observed no difference between these two conditions, indicating that FTSJ1-mediated Um34 modification regulates UGA
141 recoding efficiency independent of selenium availability. Z-score was used to compare relative differences in recoding
142 efficiency (Figure 3D). We observed a similar decrease in UGA recoding efficiency in WT A375 melanoma cells without
143 selenium as *FTSJ1*-KO cells, highlighting the role of Um34 modification in UGA readthrough.
144
145 We plotted the Cumulative Fraction of RPFs across each selenoprotein transcript to assess ribosomal accumulation.
146 Comparing WT A375 melanoma cells in the presence and absence of selenium (30nM NaSe), we found that a subset of
147 selenoproteins showed an increase in ribosomal accumulation 5' of the Sec UGA codon when selenium was depleted
148 (Extended Figure 4A). *FTSJ1*-KO cells had a similar ribosomal accumulation 5' of the Sec UGA codon in this subset of
149 transcripts (Extended Figure 4B). Interestingly, SELENOK was not affected by the absence of selenium in WT A375
150 melanoma cells but showed significant ribosomal accumulation in *FTSJ1*-KO cells. The opposite was true for SELENON,
151 which showed some accumulation of ribosomes in WT A375 melanoma cells without selenium but was not affected by
152 *FTSJ1*-KO. TXNRD1, TXNRD2, SELENOI and SELENOS were unaffected by either absence of selenium or FTSJ1 loss, however
153 these proteins all contain the Sec UGA codon at the 3' end of the transcript (Extended Figure 5A and B). Interestingly,
154 when we plotted the non-cumulative RPF counts for each selenoprotein, we saw that loss of FTSJ1 caused accumulation
155 of ribosomes 5' of the Sec UGA, even on proteins such as TXNRD1 and SEPHS2 which previously appeared to be
156 unaffected by the loss of FTSJ1 (Extended Figure 6). Taken together, these results suggest that FTSJ1-mediated Um34
157 modification increases the efficiency of UGA readthrough, independent of the specific selenoprotein.
158
159 *FTSJ1 regulates Sec insertion independent of selenium*
160 We assessed endogenous selenoprotein levels in two different *FTSJ1*-KO melanoma cell lines, A375 and SK-MEL2.
161 Strikingly, most selenoproteins were decreased in both A375 and SK-MEL2 *FTSJ1*-KO melanoma cell lines (Figure 3E),
162 especially those involved in the antioxidant response (GPX1, GPX4, MSRB1 and SELENOH). SELENOS was only decreased

163 in A375 melanoma cells and SELENOM was only decreased in SK-MEL2 cells, suggesting a difference in selenoprotein
164 regulation depending on genetic background of the cells. Other proteins such as SELENOK, SELENON, SELENOO, TNXRD1
165 and SEPHS2 were not significantly affected by FTSJ1 loss in either cell line, although SELENOK and SELENON did show a
166 smaller isoform in SK-MEL2 cells which could indicate a truncated protein where the Sec-coding UGA is read as a stop
167 codon. Importantly, these changes were not observed at the mRNA level (Extended Figure 3B), emphasizing that loss of
168 Um34 leads to a translational defect of a subset of selenoproteins. Strikingly, upon loss of FTSJ1 we also saw a decrease
169 in SECISBP2, suggesting FTSJ1 may be involved in stabilizing the SECIS-binding protein complex to promote selenoprotein
170 translation, however this finding warrants further study.
171
172 To address whether FTSJ1 is sufficient to drive translation of endogenous selenoproteins when selenium is limiting, we
173 established a system to decrease selenium levels in cells without complete depletion. Due to the variable presence of
174 selenium in serum albumin (150-300nM)[39], A375 and SK-MEL2 melanoma cells were cultured in either normal (10%) or
175 reduced (2%) FBS levels, with or without selenium supplementation (30nM NaSe). In normal growth conditions (10% FBS,
176 no NaSe), cells had basal levels of selenoproteins GPX1, GPX4 and TXNRD1 (Extended Figure 3C). Growth in 2% FBS, and
177 therefore reduced selenium, led to a decrease in selenoproteins, while selenium supplementation increased
178 selenoprotein levels in both conditions in A375 and HEK-293T cells (Extended Figure 3C). Unlike their proteins, TXNRD1
179 and GPX4 mRNAs did not change when levels of selenium were varied, suggesting levels of selenium affect translation
180 but not transcription of selenoproteins (Extended Figure 3D). GPX1 mRNA, which is regulated through nonsense
181 mediated decay[40] showed a modest reduction with reduced FBS but did not increase with selenium supplementation.
182 Compared to control cells, FTSJ1-overexpressing cells had increased antioxidant selenoproteins, GPX1 and GPX4, both in
183 high and low levels of selenium, whereas housekeeping selenoproteins TXNRD1 and SEPHS2 and selenoprotein machinery
184 such as SEPSECS were unaffected by FTSJ1 overexpression (Figure 3F).
185
186 To confirm the role of Um34 in selenoprotein translation, we assessed UGA readthrough in *FTSJ1*-knockout cells using the
187 gROSI reporter. Translation of the seleno-GFP was increased in the presence of selenium, but this increase was abolished
188 in *FTSJ1*-knockout cells (Figure 3G). Conversely, overexpression of FTSJ1 caused a significant increase in translation of
189 gROSI independent of selenium levels, indicating that Um34 modification is sufficient for readthrough of UGA as a

190 selenocysteine (Figure 3H). To specifically assess Sec-insertion into selenoproteins, we adapted a method for
191 selenocysteine-specific labeling and enrichment[41, 42]. Selenocysteine residues are labelled with a biotinylated probe at low
192 pH, followed by avidin-immunoprecipitation of the selenocysteine-containing proteins (Sec-IP). As proof of concept, we
193 blotted for known selenocysteine proteins GPX4, SELENOS, SEPHS2 and TXNRD1, in the presence of biotin and selenium,
194 and for the non-selenocysteine containing protein, SECISBP2, as a negative control. (Extended Figure 3E). Next, we
195 performed Sec-IP on Control and *FTSJ1*-KO A375 melanoma cells and found that some selenoproteins, such as GPX1, GPX4,
196 SELENOK, SELENOS were pulled down less in the absence of FSTJ1 (Extended Figure 3F). To confirm that the increase in
197 selenoprotein levels upon FTSJ1 overexpression is due to increased UGA readthrough as a selenocysteine, we performed
198 Sec-IP of control and FTSJ1-overexpressing A375 melanoma cells in the absence and presence of selenium. Even without
199 selenium, FTSJ1-overexpressing cells exhibit as much insertion of Sec into GPX4 and SELENOS as control cells with
200 selenium supplementation (Extended Figure 3G). TXNRD1, traditionally thought to be a housekeeping selenoprotein, did
201 not respond to FTSJ1 overexpression. These data demonstrate that FTSJ1 is both necessary and sufficient for recoding of
202 the UGA as selenocysteine in a subset of selenoproteins and highlight the translational hierarchy that exists among
203 different selenocysteine proteins.
204
205 *Um34 protects cancer cells from oxidative stress*
206 Given that Um34 is required for translation of antioxidant selenoproteins and its levels increase in response to oxidative
207 stress, we hypothesize that Um34 and FTSJ1 are required for the oxidative stress response. Surprisingly, there was no
208 increase in oxidative stress levels under normal growth conditions in FTSJ1-deficient melanoma cell lines, and only SK-
209 MEL2 showed increased lipid peroxidation (Extended Figure 7A-C). FTSJ1-deficient cells were more sensitive to
210 prooxidant Pyocyanin both with and without selenium supplementation. However, sensitivity to Pyocyanin greatly
211 increased in both control and *FTSJ1*-KO cells in the absence of selenium, suggesting a crucial role for selenoproteins in the
212 antioxidant response (Figure 4A-D). FTSJ1-deficient cells were also sensitive to ferroptosis, a form of cell death caused by
213 lipid peroxidation, when treated with RSL3 (Extended Figure 7D and E). Overexpression of FTSJ1 protected cells from
214 oxidative stress in the presence of selenium (Figure 4E and F). In the absence of selenium, overexpression of FTSJ1 had
215 no effect, supporting that FTSJ1-driven antioxidant response is dependent on synthesis of selenoproteins (Figure 4G and
216 H). To demonstrate that the sensitivity to oxidative stress was FTSJ1-dependent, we performed rescue experiments and

217 observed that overexpressing *FTSJ1* can partially rescue sensitivity to oxidative stress both in the presence and absence
218 of selenium (Figure 4I and J, Extended Figure 7F and G). FTSJ1 can similarly partially rescue sensitivity of *FTSJ1*-KO cells to
219 ferroptosis induced by RSL3 treatment (Extended Figure 7H and I). Partial rescue is likely due to limiting levels of binding
220 partner WDR6 and insufficient levels of charged $tRNA^{Sec}$. In support of this, overexpression of wild type $tRNA^{Sec}$ increased
221 cell survival under oxidative stress in the absence of selenium (Figure 4K and L and Extended Figure 7J and K), supporting
222 the fact that $tRNA^{Sec}$ may be limiting especially when selenium is depleted. To confirm that this effect is due to the Um34
223 modification, we overexpressed mutant $tRNA^{Sec}$ C65G - a patient mutation shown to specifically affect translation of
224 stress-related selenoproteins due to loss of Um34 and modifications within the anticodon loop[43,44]. Our data show that
225 $tRNA^{Sec}$ C65G is unable to rescue oxidative stress sensitivity. Consistent with this data, we found that overexpression of
226 wild type Sec tRNA leads to an increase in Um34 levels on $tRNA^{Sec}$ while overexpression of C65G mutant Sec tRNA had
227 no significant effect on Um34 levels (Extended Figure 7L). Finally, to demonstrate oxidative stress sensitivity was not
228 dependent on other FTSJ1-modified tRNAs, we overexpressed either tRNA Phe^{GAA} or Trp^{CCA}, and found neither had an
229 effect on oxidative stress resistance with or without selenium (Extended Figure 7M-P, Extended Figure 8A-D). These data
230 confirm that FTSJ1 is both necessary and sufficient for oxidative stress resistance and that this resistance is specific to
231 $tRNA^{Sec}$ containing Um34.
232
233 *Micrometastases have higher oxidative stress and Sec biosynthesis*
234 Given the central role of oxidative stress in metastatic colonization, we explored selenoprotein translation in metastasis
235 using a patient-derived xenograft (PDX) model of melanoma metastasis, in which patient melanomas transplanted into
236 NSG mice recapitulate metastatic behavior of the tumor observed in patients[45]. Using two patient tumors with different
237 driver mutations, M481 (BRAF V600E) and M405 (NRAS Q61R), we measured levels of both cytoplasmic and
238 mitochondrial oxidative stress levels in micrometastatic (<0.2mm), macrometastatic (>0.2mm) and primary
239 subcutaneous tumors. Micrometastases had significantly higher levels of oxidative stress in both subcellular
240 compartments compared to macrometastases or primary tumors (Figure 5A). Increase in oxidative stress in micro and
241 macrometastatic lesions was mirrored by a significant increase in the mRNAs for major components of selenocysteine
242 biosynthesis machinery such as PSTK, SEPSECS, ALKBH8, SECISBP2 and SECp43 (Figure 5B). In contrast, we did not see
243 significant transcriptional differences in selenoprotein mRNA levels between micrometastases, macrometastases and

244 primary subcutaneous tumors (Extended Figure 9A, Supplementary Table 3). However, we did observe significant
245 upregulation of certain selenoproteins in metastatic nodules compared to the primary tumors (Figure 5C and D),
246 consistent with the model that selenoprotein translation increases as a protective mechanism against oxidative stress.
247 Overall, our data suggest a translational mechanism for the upregulation of selenoproteins during metastasis. Levels of
248 precursor $tRNA^{Sec}$ were not changing, however levels of mature $tRNA^{Sec}$ were slightly elevated in metastases compared
249 to the primary tumor, similarly suggesting a translational mechanism of selenoprotein upregulation (Extended Figure 9B
250 and C). Levels of FTSJ1 were also elevated in metastases, increasing more in micrometastases compared to
251 macrometastases (Figure 5C and 5E-F). Consistent with FTSJ1 increase, levels of Um34 modification on $tRNA^{Sec}$ were also
252 elevated in metastatic nodules compared to the primary tumor (Figure 5G).
253
254 To confirm translational upregulation of selenoproteins in metastasizing melanoma cells, we transplanted A375
255 melanoma cells expressing the gROSI reporter with no UTR, GPX1 SECIS or GPX4 SECIS. By quantifying GFP signal in
256 metastatic nodules compared to primary tumors, we found that metastases had significantly higher seleno-GFP with
257 either GPX1 SECIS or GPX4 SECIS, demonstrating increased UGA readthrough as a selenocysteine in metastasizing
258 melanoma cells (Extended Figure 9D and E). Overall, these data indicate that metastatic lesions experience higher levels
259 of oxidative stress and have increased selenocysteine biosynthesis, UGA readthrough, and translation of some
260 selenocysteine proteins.
261
262 *Um34 promotes metastasis in vivo.*
263 To determine if FTSJ1 and therefore $tRNA^{Sec}$ Um34 modification are necessary for metastasis, we transplanted FTJS1 KO
264 A375 melanoma cells co-expressing luciferase subcutaneously into immunocompromised mice and measured both
265 primary tumor growth as well as overall metastatic burden in the organs. Loss of *FTSJ1* lead to significant decrease in
266 metastasis without any impact on the growth of the primary tumor (Figure 6A and B, Extended Figure 10A). MeWo
267 melanoma cells expressing *FTSJ1*-targeting shRNAs exhibited the same phenotype when transplanted *in vivo* with
268 knockdown of *FTSJ1* causing a decrease in metastatic burden without impacting growth of the primary tumor (Figure 6C
269 and D, Extended Figure 10B-D). Depleting FTSJ1 using shRNAs in two different PDX melanoma tumors, M405 and M481,
270 also did not change primary tumor growth but significantly decreased metastatic spread into the organs (Figure 6E-H,

271 Extended Figure 10E and F). A significant change in circulating tumor cell (CTC) frequency was not seen likely due to low
272 levels of CTCs in the PDX model and a potential increased dependence on oxidative stress resistance after metastatic
273 seeding. To address whether FTSJ1 activity was sufficient to promote metastasis, we overexpressed FTSJ1 in A375
274 melanoma cells and transplanted them *in vivo*. *FTSJ1* overexpression had no effect on primary tumor growth but
275 increased metastatic burden in the organs of the mice (Figure 6I – J, Extended Figure 10G). The same phenotype was
276 observed when *FTSJ1* was overexpressed in a PDX tumor, M481 (Figure 6K-L, Extended Figure 10H). The second PDX
277 tumor, M405, also showed a trend towards an increase in metastasis (Extended Figure 10I - J). To assess whether FTSJ1
278 had an effect on metastatic colonization, we injected *FTSJ1*-KO cells intravenously and saw a trend towards a decrease in
279 metastasis (Extended Figure 10K). Similarly, when we transplanted FTSJ1 overexpressing cells intravenously, there was a
280 trend towards an increase in metastasis (Extended Figure 10L). We assessed whether levels of lipid peroxidation were
281 specifically affected in either FTSJ1-depleted cells or FTSJ1-overexpressing cells *in vivo*. In either case lipid peroxidation
282 markers did not significantly change in the primary tumor (Extended Figure 10M and N). These data demonstrate that
283 FTSJ1 is both necessary and sufficient for metastatic colonization *in vivo*.
284
285 **DISCUSSION**
286 Our findings reveal that Um34, a single modification of the anticodon loop on the selenocysteine tRNA, is required for
287 efficient translation of selenoproteins, promoting oxidative stress resistance and metastasis. We specifically identify
288 oxidative stress as an inducer of Um34 and selenoprotein translation independent of selenium. We characterized FTSJ1
289 as the Um34 methyltransferase by demonstrating its activity *in vitro*, showing its direct interaction with $tRNA^{Sec}$ as well
290 as selenocysteine translational machinery. Ribosomal profiling data confirm Um34 is required for efficient readthrough
291 of the UGA stop codon on all selenoproteins regardless of selenium status. We hypothesize the apparent hierarchy of
292 selenoprotein translation may be determined by other factors such as transcript and protein stability and the position of
293 the UGA stop codon, however this warrants further study.
294
295 The Um34 methyltransferase has been a long standing unknown and previous work on the mechanistic role of Um34 has
296 relied on a mutant $tRNA^{Sec}$ i^6A37G, lacking the i6A modification – a prerequisite for Um34 formation[40, 46]. No study has
297 directly uncoupled the function of i^6A from that of Um34. Over the course of this work, FTSJ1 was separately proposed

298 to be the Um34 methyltransferase[36]. Intriguingly, there were no clear selenoprotein translational effects in the Ftsj1-KO
299 adult mouse brain[47]. In contrast, we have established a functional role for Um34-mediated translation of selenoproteins
300 in oxidative stress resistance and specifically showed that Um34 modification is a *bona fide* metastatic promoter in
301 xenograft models of melanoma. Importantly, loss of Um34 specifically impacted metastatic colonization likely by
302 increasing oxidative stress resistance but is dispensable for proliferation of cancer cells in the primary tumor.
303
304 FTSJ1 is known to modify several other tRNAs, mainly $tRNA^{Phe}$ and $tRNA^{Trp}$ and its pathogenesis has been implicated in X-
305 linked intellectual disability in patients[48, 49]. Previous studies show that constitutive knockout of FTSJ1 in mice leads to
306 loss of anticodon modifications on 11 tRNAs and aberrant brain function but otherwise normal tissue development in the
307 body. Similarly, patients with mutations in FTSJ1 manifest non-syndromic X-linked intellectual disability but show no
308 dysmorphism. This work emphasized that $tRNA^{Phe(GAA)}$ was most significantly affected in the KO mouse brain which
309 correlated with impaired translation at Phe codons and neurological phenotypes but was unaffected in other adult
310 tissues[36]. Our ribosomal profiling data do not show significant changes in Phe GAA codon readthrough in *FTSJ1*-KO
311 melanoma cells, suggesting FTSJ1 activity may have phenotypic tissue specificity. Given the role of FTSJ1 in brain
312 development, it would be interesting to explore selenoprotein translation at different stages of embryonic
313 neurodevelopment. Further studies are needed to explore other physiological contexts in which $tRNA^{Sec}$ Um34 maybe
314 required, including thyroid hormone regulation, inflammation and neurodegenerative pathologies that are also
315 associated with oxidative stress dysregulation.
316
317 Given that redox dysregulation is a hallmark to cancer, it is possible that effects of Um34 loss are more pronounced in
318 cancer cells. Most importantly, metastasis may represent a unique process, highly sensitive to perturbation in oxidative
319 stress, and therefore highly dependent on the antioxidant selenoproteome regulated by Um34 for metastatic
320 colonization. We observed sensitivity to RSL3 *in vitro* upon KO of *FTSJ1*; however, levels of lipid peroxidation were not
321 elevated at baseline. Sensitivity may be due to reduced levels of GPX4, the target of RSL3, however they may be sufficient
322 to maintain lipid peroxidation levels at baseline where cells are cultured under optimal conditions. Additional work is
323 needed to determine if *FTSJ1*-KO leads to increased ferroptosis *in vivo*, where the metastatic cascade generates vastly
324 different stress conditions.

325

326 Our work highlights Um34 as a regulatory node that specifically controls the antioxidant response through translation of
327 selenoproteins. It will be particularly important to explore the molecular synergy between how selenium levels and
328 oxidative stress regulate Um34-driven translation. We observe an increase in FTSJ1 protein expression in response to
329 oxidative stress and selenium supplementation as well as in metastatic nodules. ALKBH8, which generates the Um34-
330 precursor, mcm^5U, is also induced upon oxidation[30]. It is possible that together these Sec tRNA-modifying enzymes
331 coordinate the selenium and oxidation status of the cell to promote translation of selenoproteins. We propose that these
332 enzymes have the potential to be potent therapeutic targets for metastatic disease. Although previous reports have
333 identified other tRNAs as drivers of metastasis[50], these code for common amino acids that are also required by normal
334 tissues and are difficult to drug. In contrast, tRNA modifying enzymes such as FTSJ1 and ALKBH8 may represent effective
335 drug targets with minimal toxicity to normal tissues.

336

337 **METHODS**

338 **Ethics statement**

339 This study complies with all relevant ethical regulations. All experiments were performed according to protocols
340 approved by the animal use committees at Weill Cornell Medicine (Protocol 2017-0033).

341

342 **Reagents and Equipment**

343 Commercially available reagents were used without further purification.

344

345 **Cell lines and culture conditions**

346 A-375 (CRL-1619), SK-MEL-2 (HTB-68), SK-MEL-28 (HTB-72), MeWo (HTB-65), HeLa (ATCC CCL-2) and HEK-293T (ATCC CRL-
347 3216) cell lines were purchased from ATCC. All cells were maintained in DMEM containing 4.5g/L glucose and L-glutamine
348 without sodium pyruvate (Corning 10-017-CV). All media was supplemented with 10% Fetal Bovine Serum (Thermo Fisher
349 Scientific) and 1% Penicillin Streptomycin (Corning). All cell lines were grown at 37°C with 5% CO_2 and tested for
350 mycoplasma.

351

352 **Plasmid Construction**

353 miR-E shRNA knockdown constructs were generated by the splashRNA program and ordered from Invitrogen as oligos.
354 Hairpins were ligated (T4 Ligase, NEB) into SiREP lentiviral plasmid behind an SFFV promoter and EGFP fluorescent
355 protein using XhoI and EcoRI sites. For overexpression constructs, the coding sequences of specific proteins were
356 ordered as gene fragments (IDT) with an N-terminus Kozack sequence and 3xFLAG or 3xHA tag. (C-terminus tag: FTSJ1,
357 SECp43, N-terminus tag: SBP2, EEFSEC, WDR6). Constructs were ligated (In-Fusion HD, Takara) into pLenti vector behind
358 an EFS promoter using BamHI and NsiI sites. A cleavable P2A site links the protein expression to a fluorescent protein
359 tag. CRISPR knockout sgRNA sequences were generated using Geneious cloning software and ordered as single stranded
360 oligos from IDT. Vector backbones were kindly provided by Lukas Dow, and all plasmids were sequence verified.

361

362 **Lentiviral transduction and generation of stable cell lines**

363 For virus production, 0.9μg of plasmid was combined with 1μg of packaging plasmids (0.4μg pMD2G and 0.6μg psPAX2)
364 and transfected into HEK 293T cells using Polyjet (SignaGen) according to manufacturer's instructions. Fresh media was
365 added the following day and viral supernatants were collected 72hr after transfection and filtered through a 0.45μM
366 filter. Approximately 1 million cells were infected with viral supernatant and 10μg/mL polybrene (Sigma-Aldrich). Cells
367 then underwent antibiotic selection with puromycin, hygromycin or blasticidin (Inviogen) depending on the antibiotic
368 resistance of each plasmid. For CRISPR knockout, cells stably-expressing Cas9 were infected with the gRNA construct. To
369 generate single clones, cells were diluted and plated into a 10cm dish. Glass rings were used to isolate single cells and
370 grow colonies. All single clones were verified by western blot analysis and Synthego genomic DNA sequencing.

371

372 **Selenium supplementation and depletion in cell culture**

373 Sodium selenite (VWR) was used to supplement selenium in cell culture. "Full media" constitutes DMEM media with 10%
374 FBS – which contains trace levels of selenium bound to albumin. 2% FBS in DMEM was used to lower selenium levels in
375 media without depleting cells of FBS. To achieve 0nM Se, DMEM was combined with Ham's F12 nutrient mix (Thermo
376 Scientific) at a 1:1 ratio with no FBS present. 30nM sodium selenite was then added for selenium supplementation in
377 DMEM/F12 media.

378

379 **tRNA biotin enrichment**

380 Small RNA was extracted from cells or tissue using RNAzol RT (Molecular Research Center) according to manufacturer's
381 instructions. tRNA enrichment was performed as previously described[12]. Briefly, M270 magnetic Streptavidin beads were
382 washed then incubated with a biotin-labelled oligo specific to the 3' end of the tRNA for 30min at RT with gentle shaking.
383 Beads were then washed to remove excess oligo and resuspended in in 6xSSC buffer (Fisher Scientific). 40-60µg small
384 RNA was also resuspended in 6xSSC buffer. The beads and RNA were incubated separately for 5 min at 75°C and then
385 combined for an additional 5 min incubation. The combined beads and small RNA were then incubated for 40 min at RT
386 with gentle shaking. Beads were then washed three times with 3x SSC, two times with 1x SSC, and several times with 0.1x
387 SSC until the absorbance at 260nm of the wash supernatant was 0. tRNA was eluted in 0.1x SSC by incubating the beads
388 with buffer at 65°C for 3-4 min. tRNA was then precipitated by adding 1µL glycogen (Sigma-Aldrich) and 300mM NaOAc
389 to the tRNA elution followed by the addition of 4x volume 100% ethanol. Samples were then stored at -80°C overnight.

390

391 **Analysis of nucleoside modification by LCMS**

392 Ethanol-precipitated tRNA was pelleted by centrifugation for 15min at 10,000xg. After washing with 70% ethanol, the
393 pellet was resuspended in 20µL H_2O. tRNA samples were enzymatically hydrolyzed to nucleosides as previously
394 described[51]. Briefly, tRNA was then boiled at 100°C for three minutes and then immediately placed in an ice water bath to
395 cool. Two units Nuclease P1 (NEB) were added with 1/10 volume 0.1M ammonium acetate pH 5.3 for two hours at 45°C.
396 0.002 units of venom phosphodiesterase (Sigma Aldridge) were added with 1/10 volume 1M ammonium bicarbonate and
397 incubated for 2 hours at 37°C. 0.5 units alkaline phosphatase (NEB) was then added and incubated for one hour. Once
398 digestion was complete, the full volume was transferred to a 10kDa centrifugal filter (Pall Nanosep OD010C34) to remove
399 enzymes. Columns were centrifuged for 8 min at 14,000xg at 4°C. Digested nucleosides were then used directly for LC-
400 MS analysis on an Agilent ZORBAX SB-C18, 2.1 X 150mm, 3.5µm column. Chromatography and Mass Spectrometry
401 methods were performed exactly as described in Songe-Moller et al, 2010 on an Agilent HPLC 1290 connected to an
402 Agilent QQQ[12].

403

404 **Analysis of GFP selenocysteine reporter by flow cytometry**

405 The selenocysteine insertion reporter consists of a destabilized-GFP (d2GFP) as described by Corish et al[52] and a
406 selenocysteine insertion element (SECIS) from GPX1 or GPX4. This is followed by an IRES – iRFP in order to normalize GFP
407 signal to active translation levels in the cell. Both cysteines in GFP were either replaced with UGA, UAA or UAG codons to
408 mimic a UGA-selenoprotein or act as an alternate stop codon control. Cells were transduced with lentiviral constructs
409 containing the reporter and cells were then selected with hygromycin (Invivogen) for one week. GFP and iRFP levels were
410 quantified by flow cytometry on an Attune NxT (Invitrogen). Analysis was completed with FlowJo software and GFP
411 signal was normalized to iRFP signal.

412

413 **Real- Time PCR Quantification of tRNA and mRNA**

414 tRNA and mRNA were extracted using a classic Trizol-chloroform RNA extraction. Reverse transcription was performed
415 using iScript cDNA synthesis kit (Rio-Rad) as described by manufacturer. cDNA was then diluted and used for qPCR
416 analysis with SYBR Green PCR master mix (Thermo Fisher). IDT online primer design tool was used to generate qPCR
417 primers and UCSC In-Silico PCR database was then used to verify human-specificity of primers. qPCR analysis was
418 performed on an Applied Biosystems QuantStudio 6 Real-Time PCR System. All targets were normalized to Actin or U6
419 snRNA in a standard ΔΔCt analysis.

420

421 **Immunoprecipitation of protein complexes**

422 Cell lines overexpressing 3xFLAG or 3xHA- tagged proteins were grown in 10cm dishes and protein lysates were made
423 with 1% Triton X-100 lysis buffer with DTT and PMSF added. Cell debris and insoluble fraction was removed by
424 centrifugation. Anti-FLAG M2 (Sigma-Aldrich) or Anti-HA (Thermo Fisher) agarose beads were washed with PBS and
425 added to the cell lysates for an overnight incubation on a rotator at 4°C. The following day, the beads were pelleted by
426 centrifugation at 1000xg at 4°C and washed 3 times with BC100 wash buffer (0.5M Tris HCl pH 7.6, 250mM EDTA, 100mM
427 KCl, 10% glycerol). Protein complexes were eluted with 3x-FLAG peptide (Sigma-Aldrich) or HA peptide (Thermo Fisher)
428 diluted to 1mg/mL in TBS. Protein eluates were then submitted for proteomic analysis or run on 4-20% Tris-Glycine
429 polyacrylamide gels for western blot analysis.

430

431 **RNA-immunoprecipitation**

432 Cells were lysed in Triton-X as described above, with the addition of 5µL ribonuclease inhibitor, RNaseOUT (invitrogen)
433 per sample to the lysis buffer. Anti-FLAG M2 agarose beads were added to the lysate for overnight enrichment. The
434 following day, beads were washed as described above and protein/RNA complexes were eluted with 1mg/mL 3xFLAG
435 peptide diluted in TBS. Proteinase K (VWR) was used to digest the protein in the eluate and RNA was extracted. Briefly,
436 PK Buffer (100mM Tris-HCl pH 7.5, 50mM NaCl, 10mM EDTA) was incubated with Proteinase K at 37°C for 20 min to digest
437 any potential RNAses present. FLAG bead supernatant was combined with 100µL Proteinase K solution and incubated for
438 20 min at 37°C. 100µL 7M Urea buffer (7M Urea, 100mM Tris-HCl pH 7.5, 50mM NaCl, 10mM EDTA) was added to the
439 reaction and incubated for an additional 20 min at 37°C. All 37°C incubations were performed on a thermomixer with
440 gentle mixing. For small RNA extraction, 700µL RNAzol RT was added to the reaction and incubated for an additional 20
441 min at 37°C. Small RNA was extracted as described by manufacturer's instructions. Small RNA was precipitated with 20µg
442 glycogen using 1M NaOAC/Ethanol extraction. cDNA was synthesized using iScript cDNA Synthesis Kit (Bio-Rad) and RNA
443 bound to protein complexes was analyzed by qPCR.

444

445 **Recombinant protein expression and purification**

446 FTSJ1 (C-6xHis) and WDR6 (N-6xHis) coding sequences were codon-optimized for e.coli bacteria and cloned separately
447 into petDuet-1 (purchased from Addgene) using the NcoI site downstream of the first T7 promoter. Plasmids were
448 transformed into One Shot BL21 (DE3) E. coli (ThermoFisher). Colonies were grown in 6mL LB ampicillin overnight. The
449 following day, cells were expanded to 1 L LB and grown until OD = 0.5-0.6. IPTG was added to 0.1mM and cells were
450 shaken overnight at 18°C and 225 RPM to allow for induction of recombinant protein. The following day, cells were
451 pelleted, washed with PBS and resuspended in lysis buffer (1% Triton X-100, 5mM imidazole in PBS) and sonicated 4x 15
452 sec at 30% duty cycle output 3 with 1 minute on ice between sonication. Lysates were centrifuged to remove insoluble
453 fraction. NaCl was added to supernatant to raise salt to 500mM. 1mL/sample Ni-NTA resin (Qiagen) was first washed with
454 lysis buffer with 500mM NaCl then beads were added to supernatant and incubated with rotation for 40 min at 4°C. Resin
455 was washed first with 40mL high salt wash buffer (10mM Tris pH 7.8, 1% Triton X-100, 50mM imidazole, 1M NaCl) then

456 20mL low salt wash buffer (0.5M Tris-HCl pH 7.6, 250mM EDTA, 50mM imidazole, 70mM KCl, 10% glycerol). Recombinant
457 proteins were eluted 4 times with 1mL elution buffer (0.5M Tris-HCl pH 7.6, 250mM EDTA, 250mM imidazole, 70mM KCl,
458 10% glycerol). Protein was concentrated using Amicon 10K centrifugal filters (Millipore). PMSF was added to all buffers
459 including PBS and DTT was also added to the elution buffer. Purification was validated using Coomassie staining and
460 western blot analysis.
461
462 ***in vitro* tRNA methyltransferase assay**
463 *in vitro* assays of FTSJ1/WDR6 2'-O-methylation of Sec tRNA was performed as previously described[35], however Sec tRNA
464 was extracted from mammalian *FTSJ1*-KO cells to provide a tRNA substrate with mcm^5U_{34} precursor. Reactions were
465 carried out at 37°C for 2hr in a 100µL reaction mixture containing 50mM Tris-HCl pH 7.5, 200mM NaCl, 10mM $MgCl_2$,
466 100µg/mL BSA, 5mM DTT, 5µM Sec tRNA, 100µM SAM with 1µM FTSJ1 and 0.2µM WDR6. tRNAs were extracted with
467 phenol/chloroform and ethanol precipitated. tRNAs were digested as described above with Nuclease P1, venom
468 phosphodiesterase and alkaline phosphatase then analyzed using HPLC-MS/MS analysis as described above.
469
470 **Selenocysteine-specific protein enrichment**
471 Utilizing the differential pKa values of Sec (5.2) and Cys (8.5), we are able to specifically label Sec residues and block Cys
472 residues in both cell lines and tissues[41, 53].Cell or tissue were lysed in MES lysis buffer pH 5.6 (50mM MES (Sigma Aldrich),
473 150mM NaCl, 1mM EDTA, 1% Triton X-100) in the presence of protease inhibitors and 0.1mM Iodoacetyl PEG2 biotin
474 (IodoAPB, Fisher Scientific). Protein was quantified and 2mg input was used for protein enrichment by rotating for 1hr at
475 RT to in 0.1mM IodoAPB to selectively label deprotonated selenocysteine residues. Protein was then precipitated with
476 methanol and the pellet was washed a couple times to remove any remaining IodoAPB. Protein pellets were then
477 resuspended in buffered 8M Urea. 5M iodoacetamide (Sigma-Aldrich) was added for 1hr at RT to selectively block
478 deprotonated cysteines. Proteins in urea were added directly to streptavidin agarose beads (Invitrogen) in PBS, 0.1% SDS
479 and rotated overnight at 4°C. The following day, beads were washed three times with 2M Urea in PBS, 0.1% SDS and then
480 three additional times in 2M Urea in PBS without SDS. For western blot analysis, beads were boiled in 1x protein loading
481 buffer at 95°C for 5 minutes.

482

483 **Ribosomal Sequencing**

484 The Ribo-seq libraries were generated as previously described with following modifications (McGlincy et al.)[38]. Cells were
485 snap-frozen and allowed to thaw on ice, then lysed in lysis buffer [50 mM Tris-HCl (pH 7.4), 150 mM NaCl, 5 mM $MgCl_2$, 1
486 mM DTT, 1% Triton X-100, 100 µg/mL cycloheximide, 100 µg/mL tigecycline, 15 U/mL DNaseI (ThermoFisher, 89836)]. RNA
487 was quantified using Qubit Broad range RNA kit (ThermoFisher, Q10211). Ribosome footprint was generated using 15 U
488 RNase I (Biosearch Technologies, N6901K) to 300 ug RNA in 200 µL reaction volume at room temperature for 45 min.
489 The ribosome was collected by ultracentrifugation and ribosome footprint was purified using TRIzol (ThermoFisher,
490 15596018). RNA was then dephosphorylated and subjected to size selection from 17-40 nt range from 15% polyacrylamide
491 TBE-Urea gel. Ribosome footprint was extracted from the gel in the extraction buffer [50 mM Tris-HCl (pH 7.0), 300 mM
492 NaCl, 1 mM EDTA, 0.25 % SDS] and subjected to rRNA depletion using Human/Mouse/Rat riboPOOL kit (Galen Molecular,
493 dp-K024-000050) by following the manufacture's instruction. rRNA-depleted ribosome footprint was precipitated in 80%
494 ethanol at -20 °C overnight. rRNA-depleted ribosome footprint was then ligated to a pre-adenylated linker (rApp-
495 WWAGATCGGAAGAGCACACGTC-3ddC). The footprint was reverse transcribed by SuperScript III reverse transcriptase
496 (ThermoFisher, 18080044) with a 5' phosphorylated primer that contains eight-nucleotide unique molecular identifiers
497 and two spacer residues (Phos-NNNNNNNNAGATCGGAAGAGCGTCGTGTA-iSp18-AA-iSp18-TAGACGTGTGCTC). cDNA was
498 run on 10% non-denaturing gel to remove the non-ligated linker and the reverse transcription primer. cDNA was the
499 circularized using CircLigase I in the presence of 1 mM ATP. The library was PCR amplified using KAPA HiFi HotStart
500 ReadyMix (FisherScientific, 50-196-5217) and NEBNext® Multiplex Oligos for Illumina® Dual Index Primers Set 1 (NEB,
501 E7600S). The library was purified twice using 1x AMPure XP Bead (BeckmanCoulter, A63881). The library was sequenced
502 for single-end 100 cycles on Illumina NextSeq 2000 or paired-end 100 cycles on Illumina NovaSeq 6000.

503

504 **Ribo-Seq Analysis**

505 Ribo-Seq reads were trimmed using Trim Galore v0.6.10 (https://github.com/FelixKrueger/TrimGalore/tree/master) to
506 remove nucleotides with low quality and adaptor contamination. Duplicated reads created by PCR amplification were
507 removed using the UMI reads and running fastq2collapse.pl and stripBarcode.pl scripts from CTK tool kit (PMID:
508 27797762). Then, non-coding RNA were removed using a custom reference genome composed by miRNA, rRNA, tRNA

509 and lncRNA sequences. miRNA sequences were downloaded from RNAcentral database (https://rnacentral.org), tRNA
510 sequences were obtained from GtRNAdb (http://gtrnadb.ucsc.edu/index.html) using High confidence GRCH38/hg38
511 tRNA sequences, lncRNA were downloaded from LNCipedia (PMCID: PMC3531107) and rRNA reference sequence was
512 built using U13369.1, NR_145819.1, NR_146144.1, NR_146151.1, NR_146117.1, X12811.1, NR_003287.4, NR_023379.1,
513 NR_003285.3 and NR_003286.4. Mapping was performed using STAR v2.7.9a (PMCID: PMC3530905) with default
514 parameters and reads that mapped to the custom reference were removed. FastQC v0.11.8 was used for quality control
515 of the remaining reads. STAR v2.7.9a was used for a second mapping step to the full human reference genome, with –
516 alignEndsType EndToEnd and –quantMode TranscriptomeSAM, using GRCh38 primary assembly genome and MANE v1.2
517 annotation file to obtain transcriptome and genome mapping coordinates.
518
519 Aligned bam files originated from mapping to the transcriptome were used as input for riboWaltz package
520 (https://doi.org/10.1371/journal.pcbi.1006169). Nucleotide base in-frame p-sites coverages were calculated to determinate
521 stalling based on downstream cumulative distribution function (CDF), to identify UGA recoding efficiency by 5' and 3'
522 footprints, and to calculate p-site codon usage. For in-frame p-site coverage quantification, reads longer than 25 pb and
523 shorter than 45 pb were kept and p-offsites were calculated for each read length using psite function in riboWaltz with
524 default arguments. Once, p-site position of each read was identified, only in-frame p-sites were kept for further analysis.
525 Mean values and cumulative fractions across the replicates in the different conditions were calculated and plotted using
526 the in-frame p-site coverage in selenoproteins.
527
528 In a similar way, UGA recoding efficiency was determined based on the obtained CDS p-site coverage. Ratio of 5' and 3'
529 coverages were calculated on fixed -X and +X bases relative to the Sec codon. Since we were using only CDS p-site values
530 and for some of the selenoproteins the distance between Sec and stop codon was short, these fixed bins were different
531 between selenoproteins (refer to the GitHub code to identify the number of bases used for each selenoprotein). Codon
532 usage of p-site was calculated using codon_usage_psite function from riboWaltz. Script used in this analysis are available
533 at https://github.com/abcwcm/piskounova_ribo.
534
535 **Tissue RNA-Sequencing**

536 RNA-seq library from primary and metastatic tumors from PDX model of melanoma metastasis was prepared by snap
537 freezing tissue in Trizol. RNA was extracted according to manufacturer's instructions using TRIzo (ThermoFisher,
538 15596018) and quantified on NanoDrop. RNA library was generated using TruSeq Stranded Total RNA Library Preparation
539 (rRNA depletion and Stranded RNA-Seq). The library was sequenced for single-end 100 cycles on Illumina NextSeq 2000.
540

541 **Tissue RNA-Seq Analysis**

542 Mouse reads from Xenograft data were removed using *bbsplit.sh* from BBMap v38.90 (BBMap - Bushnell B. -
543 sourceforge.net/projects/bbmap/) with ambiguous2=="toss" and using gencode GRCh38 human and GRCm39 mouse
544 references. Using same tools and parameters as for Ribo-Seq analysis, low quality reads and adaptors were trimmed, and
545 non-coding RNA reads were removed. In the same way, the quality control step was performed using FastQC v0.11.8 and
546 a second mapping to the full human reference genome was performed using STAR v2.7.9a and same parameters as in
547 Ribo-Seq. Using bam files of the mapped reads to the whole genome gene counts quantification of CDS regions was
548 calculated using featureCounts v 2.0.1 (PMID: 24227677). Using the obtained counts PCA analysis was performed to
549 analyze the similarities among the samples. This analysis identified significant patient donor effect (M405, M481) and
550 therefore, normalization and further differential expression analysis based on DESeq2 (PMID: 25516281) approach were
551 performed separately for M405 and M481. Wald test was applied to identify changes in Selenoproteins between primary,
552 macro and micro tumor types and adjusted p-values were based on Benjamini-Hochberg procedure.
553

554 **Analysis of cell survival under prooxidant treatment**

555 Cells were plated at 10,000 cells/well in a white TC-treated 96 well plate (Corning). The following day, DMEM/F12 media
556 with 0nM or 30nM selenium was added. After 24 hours of selenium depletion or supplementation, cells were then treated
557 with prooxidant pyocyanin (Cayman), H_2O_2 (Sigma-Aldrich) or translation inhibitor tunicamycin (Tocris). After 24 or 48
558 hours of treatment, CellTiter-Glo 2.0 (Promega) was used according to manufacturers instructions to quantify cell
559 viability.
560

561 **Lentiviral transduction of human melanoma cells**

562 Patient-derived tumors M405 and M481 were derived as described in[45, 54, 55]. A lentiviral construct with luciferase and

563 dsRed (luc P2A dsRed) was used to label patient-derived melanoma cells as described in[29]. Virus was produced as
564 described above. For lentiviral transduction, 500,000 freshly dissociated melanoma cells were infected with viral
565 supernatant and supplemented with 10 µg/mL polybrene (Sigma). The following day, the media was replaced and 48hrs
566 post-infection cells were either injected subcutaneously into mice as bulk tumors or FACS sorted for positive infection.
567

568 **Cell labeling and sorting**

569 All melanoma cells in this study stably express dsRed and luciferase so that melanoma cells could be distinguished by
570 flow cytometry or bioluminescent imaging. When preparing cells for sorting by flow cytometry, cells were stained with
571 antibodies against mouse CD45 (30-F11-VioletFluor, Tonbo), mouse CD31 (390-VioletFluor, eBiosciences), Ter119 (Ter-119-
572 VioletFluor, Tonbo) and human HLA-A, -B, -C (BD Biosciences) to select live human melanoma cells and exclude mouse
573 endothelial and hematopoietic cells. Antibody labelling was performed for 20 min on ice, followed by washing and
574 centrifugation. Before sorting, cells were resuspended in staining medium (L15 medium containing bovine serum albumin
575 (1 mg/mL), 1% penicillin/streptomycin, and 10mM HEPES, pH 7.4) containing 4'6-diamidino-2-phenylindole (DAPI; 5µg/mL;
576 Sigma) to eliminate dead cells from sorting. Live human melanoma cells were isolated by flow cytometry by sorting cells
577 that were positive for dsRed and HLA and negative for mouse CD45, CD31, Ter-119 and DAPI.
578

579 **Transplantation of melanoma cells**

580 After sorting, cells were counted and resuspended in staining medium with 25% high-protein Matrigel (product 354248;
581 BD Biosciences). Subcutaneous injections were performed into the right flank of NOD.CB17-*Prkdc*^{scid} *Il2rg*^{tm1Wjl}/SzJ (NSG)
582 mice (Jackson Laboratory) in a final volume of 50 µl. Both male and female mice, 5-8 weeks old were used. Sex was not
583 considered in the study design. Mice were randomized between control and experimental groups, where mice with
584 comparable age and body weight were assigned into control and experimental groups. For a standard metastasis assay,
585 100 cells were injected subcutaneously into the right flank of the mice. Tumor formation was evaluated by regular
586 palpitation of the injection site and tumors were measured weekly until any tumor in the mouse cohort reached 2.5cm in
587 its largest diameter. Mice were monitored daily for signs of distress according to a standard body condition score or
588 within 24hr of their tumors reaching 2.5 cm in diameter – whichever came first. These experiments were performed
589 according to protocols approved by the Institutional Animal Care and Use Committee at Weill Cornell Medicine (protocol

590 2017-0033). If tumor burden was found to exceed 2.5cm, mice were euthanized immediately as was allowed by the IACUC
591 protocol 2017-0033. For intravenous transplantation, 1000 A375 melanoma cells were injected into the tail vein of NSG
592 mice in 100ul of PBS. Mice were imaged weekly by bioluminescence until signal was saturated.
593
594 **Animal studies**
595 For bioluminescent imaging, mice were injected intraperitoneally with 100µL of DPBS containing D-luciferin
596 monopotassium salt (40µg/mL, Goldbio) 5 min before imaging, followed by general anesthesia with isoflurane 2 min
597 before imaging. IVIS Imaging System 200 Series (Caliper Life Sciences) with Living Image Software was used with the
598 exposure time set to 10 seconds. After imaging the whole body, mice were euthanized and individual organs were
599 dissected and imaged. The bioluminescent signal was quantified with 'region of interest' measurement tools in Living
600 Image (Perkin Elmer) software. After imaging, tumors and organs were fixed in paraformaldehyde for histopathology.
601 Studies received ethical approval by animal use committees at Weill Cornell Medicine (2017-0033).
602
603 **Circulating tumor cell analysis**
604 During imaging described above, once mice were euthanized for organ dissection, blood was also collected by cardiac
605 puncture with a syringe pretreated with citrate-dextrose solution (Sigma). Red blood cells were precipitated by Ficoll
606 sedimentation according to manufacturer's instructions (Ficoll Paque Plus, GE Healthcare). Remaining cells were washed
607 with HBSS (Invitrogen) before antibody staining as described above and flow cytometric analysis.
608
609 **Immunofluorescence staining of tissue sections**
610 Tissues were fixed in 4% paraformaldehyde for 12 h at 4 uC, embedded in paraffin, and then sectioned. Sections (10 mm)
611 were deparaffinized and then subjected to antigen retrieval for 10 minutes at 121 uC at 15 PSI in 2.94 g/L sodium citrate
612 (pH 6; Sigma Aldrich, 61332-04-3). Sections were permeabilized in PBS with 0.4% Triton X-100 (PBT) and 1% bovine serum,
613 for 10 min, and blocked in 5% bovine serum in PBT for 45 min at room temperature. Sections were then stained with
614 primary antibodies overnight at 4uC: FTSJ1 (A7967, ABclonal; 1:250), GPX1 (A11166, ABclonal; 1:250), GPX4 (52455S, Cell
615 Signaling; 1:250), MSRB1 (A6737, ABclonal; 1:250), Seleno F (SEP15) (A7967, Abcam; 1:250), SELENOH (HPA048362, Atlas
616 Antibodies; 1:250), SELENOK (HPA008196, Atlas Antibodies; 1:250), SELENO S (VIMP-1) (15160S, Cell Signaling Technology;

617 1:250), TXNRD1 (15140S, Cell Signaling Technology; 1:250), GFP (13970, abcam, 1:1000) in PBS with 0.1% Triton X-100 and 1%
618 bovine serum. The next day, sections were washed in PBS with 0.1% Triton X-100 and 1% bovine serum and stained with
619 secondary, either goat anti-rabbit antibody (A-21244, Invitrogen; 1:500) or goat anti-chicken (ab150169, abcam; 1:1000),
620 for 1 hour in the dark at room temperature. Sections were washed with PBS with 0.1% Triton X-100 and 1% bovine serum
621 with DAPI (1:1500) for four minutes in the dark at room temperature and mounted for imaging. Fluorescent signal was
622 analyzed and quantified using QuPath v0.4.3 software.
623

624 **Statistics and Reproducibility**

625 No statistical methods were used to predetermine sample size but we used adequate numbers of samples that would
626 provide statistically significant results based on our previous experience with these tumor models. The data in all figure
627 panels reflect several independent experiments as indicated in figure legends. Variation is always indicated using
628 standard deviation. For analysis of statistical significance, when only two conditions were compared a two-sided unpaired
629 t-test was used, unless otherwise indicated. For comparison of multiple conditions, one-way ANOVA was used for multiple
630 comparisons, unless otherwise indicated. P value of <0.05 was considered statistically significant. Data was assumed to
631 be normally distributed, but this was not formally tested. Individual data points are shown where appropriate. All *in vivo*
632 experiments were randomized to each experimental cohort. The number of mice used is indicated in figure panels. Any
633 mice that died before the end of the experiment due to opportunistic infection, the data from these mice were excluded.
634 No blinding was used in any experiment. Otherwise no data was excluded from the analyses. Further information on
635 research design is available in the Nature Research Reporting Summary linked to this article.
636

637 **Data Availability**

638 Ribosomal Sequencing and RNA-sequencing data that support the findings of this study have been deposited in the Gene
639 Expression Omnibus (GEO) under accession codes GSE270971 and GSE270976. Mass spectrometry data for Proteomics
640 as well as nucleoside modification analysis have been provided as Supplementary Data files.
641 Source data for have been provided as Source Data files. All other data supporting the findings of this study are available
642 from the corresponding author on reasonable request by email. Requests will be processed within 30 days.
643

644 **Code availability**

645 All custom scripts used in this study are deposited at https://github.com/abcwcm/piskounova_ribo

646

647 **ACKNOWLEDGEMENTS**

648 This work was supported by American Cancer Society (EP), Elsa U. Pardee Foundation Grant (EP) and Feldstein Medical
649 Research Foundation Award (EP). LN is supported by Ruth L. Kirschstein Predoctoral Individual National Research Service
650 Award.

651

652 **AUTHOR CONTRIBUTIONS**

653 LN designed and performed experiments, analyzed data, and wrote the paper. KC, ID, MZ, GC, RH and KA performed
654 experiments and analyzed data. LED supervised CRISPR/Cas9 experiments and provided reagents. SM and SJ designed,
655 performed and supervised Ribo-Seq experiments. MA, PZ and DB designed, performed and supervised Ribo-Seq and RNA-
656 seq data analysis. EP designed, performed, and supervised experiments, analyzed data, supervised data analysis, and
657 wrote the paper.

658

659 **COMPETING INTERESTS**

660 LED is an advisor and holds equity in Mirimus Inc. and is a consultant for Volastra Therapeutics and Frazier Healthcare
661 Partners. The other authors have no conflicts to disclose.

662

663 **FIGURE LEGENDS**

664

665 **Figure 1: Selenoprotein translation and tRNA^{Sec} Um34 levels increase in response to oxidative stress**

666 (A) Schematic of selenocysteine biosynthesis and selenoprotein translation. Sec is synthesized on its tRNA. The
667 tRNA is then modified at the wobble uridine and the Sec translation complex associated with the SECIS allows
668 for co-translational readthrough of UGA stop codon.

669 (B) Schematic of tRNA^{Sec} isolation and Um34 modification analysis.

670 (C) Quantification of Um34 and mcm^5U levels in A375 melanoma cells grown in DMEM/F12 medium supplemented
671 with increasing concentrations of selenium measured by LC-MS/MS. n= 3 independent biological experiments.
672 Mean +/- SD. Statistical significance assessed by two-way analysis of variance (ANOVAs) followed by Fisher LSD
673 test for multiple comparisons.
674 (D) Quantification of Um34 modification levels on $tRNA^{Sec}$ in A375 melanoma cells treated with pro-oxidant H_2O_2
675 (100μM) pyocyanin (10μM) in DMEM/F12 media in the presence or absence of 30nM NaSe. n = number of
676 independent samples is indicated in the figure. Mean +/- SD. Statistical significance assessed by one-way ANOVA
677 followed by Fisher LSD test for multiple comparisons.
678 (E) Levels of selenoproteins in A375 melanoma cells and
679 (F) SK-MEL-2 melanoma cells after treatment with NaSe (30nM) and pyocyanin (10uM). Representative from 3
680 independent experiments shown.
681 (G) Transcript levels of selenoproteins in A375 melanoma cells after treatment with NaSe and pyocyanin measured
682 by qRT-PCR. Mean +/- SD. n=3 independent biological experiments. Statistical significance assessed by two-way
683 analysis of variance (ANOVA) with each condition compared to selenium deficient cells in the DMSO control
684 condition. *p-values: SELENOP Control – Se vs Pyocyanin – Se P=0.0308; SELENOP Control – Se vs Pyocyanin +
685 Se P=0.0210. EEFSEC Control – Se vs Control + Se P= 0.0487; EEFSEC Control – Se vs Pyocyanin + Se P=0.0407.
686 (H) Schematic of the split-seleno-GFP reporter - GFP Reporter Of Selenocysteine Insertion (gROSI).
687 (I) Flow cytometry analysis of split-seleno-GFP reporter (gROSI) expression with different combinations of stop
688 codons UAA or UGA and with No UTR or SECIS from GPX4, in the presence or absence of selenium (30nM NaSe)
689 in A375 melanoma cells. n = 3 independent biological experiments, Mean +/- SD; representative experiment
690 shown; two-sided unpaired t-test,
691 (J) Flow cytometry analysis of GFP fluorescence of gROSI variants without a 3'UTR, with a GPX4 SECIS and with a
692 GPX1 SECIS treated with Pyocyanin (10uM) and NaSe (30nM). n=3 independent biological experiments, Mean +/-
693 SD. Statistical significance measured by two-way ANOVA followed by Fisher LSD test for multiple comparisons.
694]
695 **Figure 2: FTSJ1 is the Um34 methyltransferase for $tRNA^{Sec}$**
696 (A) Alignment schematic of FTSJ1 and its homologs

697 (B) Co-immunoprecipitation assay of the interaction between HA-tagged FTSJ1 and FLAG-tagged EEFSEC, compared
698 to FLAG-tagged Scarlet-expressing control vector co-expressed in A375 melanoma cells. Representative from 3
699 independent experiments shown.
700 (C) Schematic of RNA-immunoprecipitation.
701 (D) Levels of $tRNA^{Sec}$ bound to FLAG-tagged Renilla, wild type and A26P-mutant FTSJ1, ALKBH8 and EEFSEC by qRT-
702 PCR. n = 3. Mean +/- SD of 3 independent replicates. Two-sided unpaired t-test.
703 (E) Levels of $tRNA^{Sec}$ bound to FLAG-tagged Renilla, FTSJ1 and WDR6 by qRT-PCR. n=3 independent replicates. Mean
704 +/- SD of 3 independent replicates. Two-sided unpaired t-test.
705 (F) Western blot analysis of FTSJ1 and selenoprotein GPX1 levels in control and *FTSJ1* knockout A375 melanoma cell
706 lines. Representative from 5 independent experiments shown.
707 (G) Quantification of Um34 modification levels on $tRNA^{Sec}$ from control and *FTSJ1* knockout A375 melanoma cell lines
708 measured by LC-MS/MS. Mean +/- SD. n = 3 independent biological experiment. One-way analysis of variance
709 (ANOVA) followed by Dunnett's tests for multiple comparisons.
710 (H) Western blot analysis of overexpression of control Renilla luciferase, wild type and mutant A26P FTSJ1 and
711 selenoprotein GPX4 in A375 melanoma cell lines. Representative from 3 independent biological experiments
712 shown.
713 (I) Quantification of Um34 modification levels on $tRNA^{Sec}$ in A375 melanoma cells overexpressing control Renilla
714 luciferase, wildtype and A26P mutant FTSJ1 measured by LC-MS/MS. Mean +/- SD. n = 3-4 independent replicates.
715 Statistical significance assessed by one-way analysis of variance (ANOVA) followed by Dunnett's tests for
716 multiple comparisons.
717 (J) Quantification of Um34 and mcm^5U levels on $tRNA^{Sec}$ in Control and *FTSJ1*-KO A375 melanoma cells grown in
718 DMEM/F12 medium with and without selenium (30nM) measured by LC-MS/MS. Mean +/- SD. n=2 independent
719 biological experiments.
720 (K) Quantification of Um34 levels on $tRNA^{Sec}$ in an in vitro methyltransferase assay measured by LC-MS/MS. Mean
721 +/- SD. n= 2 independent biological experiments.
722
723 **Figure 3: Um34 regulates UGA recoding efficiency in a subset of selenoproteins involved in oxidative stress**

724 (A) UGA Recoding Efficiency (Ratio of RPF 3' to Sec UGA/RPF 5' to Sec UGA) of selenoproteins in WT A375 melanoma
725 cells in the absence and presence of selenium (30nM NaSe). n=3 independent replicates per group. Pearson
726 Correlation.
727 (B) UGA Recoding Efficiency of selenoproteins in Control and *FTSJ1*-KO A375 melanoma cells in the presence of
728 selenium (30nM NaSe). n=3 independent replicates per group. Pearson Correlation.
729 (C) UGA Recoding Efficiency of selenoproteins in *FTSJ1*-KO A375 melanoma cells in the absence and presence of
730 selenium (30nM NaSe). n=3 independent replicates per group. Pearson Correlation.
731 (D) Z-score values of UGA recoding efficiency comparing WT A375 melanoma cells without selenium, WT A375
732 melanoma cells with selenium (30nM NaSe) and *FTSJ1*-KO A375 melanoma cells with selenium (30 nM NaSe). n=3
733 independent replicates per group.
734 (E) Western blot analysis of selenoprotein levels in Control and *FTSJ1*-KO A375 and SK-MEL-2 melanoma cells grown
735 in normal (10% FBS) media. Representative from 3 independent biological experiments shown.
736 (F) Western blot analysis of selenoproteins in normal (10% FBS), selenium-depleted (2% FBS) and supplemented
737 conditions (10% + 30nM NaSe and 2% + 30nM NaSe) in A375 melanoma cell line overexpressing either control
738 Renilla or FTSJ1. Representative from 2 independent biological experiments shown.
739 (G) Flow cytometry analysis of seleno-GFP reporter (gROSI) expression in control and *FTSJ1*-KO A375 melanoma cells
740 with and without selenium (30nM). Mean +/- SD of 3 independent replicates; representative experiment shown;
741 One-way analysis of variance (ANOVA) followed by Dunnett's tests for multiple comparisons (two-sided).
742 (H) Flow cytometry analysis of seleno-GFP reporter (gROSI) expression in control Renilla-overexpressing or FTSJ1-
743 overexpressing A375 melanoma cells. Mean +/- SD of 3 independent biological experiments; representative
744 experiment shown; One-way analysis of variance (ANOVA) followed by Dunnett's tests for multiple comparisons
745 (two-sided).
746
747 **Figure 4: Um34 modification protects cancer cells from oxidative stress**
748 (A-B) Cell survival of Control and *FTSJ1*-KO A375 (A) and SK-MEL-2 (B) melanoma cells under pyocyanin treatment in
749 selenium-supplemented conditions. n = 3 independent culture experiments. Mean +/- SD. Representative of 3

750 independent experiments. Statistical difference between IC50 values analyzed by Extra-Sum-of-Squares F-Test (two-
751 sided).
752 (C-D) Cell survival of Control and *FTSJ1*-KO A375 (C) and SK-MEL-2 (D) melanoma cells under pyocyanin treatment in
753 selenium-depleted conditions. n = 3 independent culture experiments. Mean +/- SD. Representative of 3 independent
754 experiments. Statistical difference between IC50 values analyzed by Extra-Sum-of-Squares F-Test (two-sided).
755 (E-F) Cell survival of Control and FTSJ1 overexpressing A375 (E) and SK-MEL-2 (F) melanoma cells under pyocyanin
756 treatment in selenium-supplemented conditions. n = 3 independent culture experiments. Representative of 3
757 independent experiments. Mean +/- SD. Statistical difference between IC50 values analyzed by Extra-Sum-of-Squares F-
758 Test (two-sided).
759 (G-H) Cell survival of Control and FTSJ1 overexpressing A375 (G) and SK-MEL-2 (H) melanoma cells under pyocyanin
760 treatment in selenium-depleted conditions. n = 3 independent culture experiments. Mean +/- SD. Representative of 3
761 independent experiments. Statistical difference between IC50 values analyzed by Extra-Sum-of-Squares F-Test (two-
762 sided).
763 (I) Cell survival of Control and *FTSJ1*-KO A375 melanoma cells with and without FTSJ1 overexpression treated with 25 uM
764 Pyocyanin in the presence of selenium. n = 3 independent culture experiments. Mean +/- SD. Representative of 3
765 independent experiments. One-way ANOVA followed by Tukey test for multiple comparisons.
766 (J) Cell survival of Control and *FTSJ1*-KO A375 melanoma cells with and without FTSJ1 overexpression treated with 25 uM
767 of Pyocyanin in the absence of selenium. n = 3 independent culture experiments. Mean +/- SD. Representative of 3
768 independent experiments. One-way ANOVA followed by Tukey test for multiple comparisons.
769 (K) Cell survival of Control, WT $tRNA^{Sec}$ and C65G-mutant $tRNA^{Sec}$ overexpressing A375 melanoma cells treated with 25uM
770 of Pyocyanin in the presence of selenium. n = 3 independent culture experiments. Mean +/- SD. Representative of 3
771 independent experiments. One-way ANOVA followed by Dunnett test for multiple comparisons.
772 (L) Cell survival of Control, WT $tRNA^{Sec}$ and C65G-mutant $tRNA^{Sec}$ overexpressing A375 melanoma cells treated with 25uM
773 of Pyocyanin in the absence of selenium. n = 3 independent culture experiments. Mean +/- SD. Representative of 3
774 independent experiments. One-way ANOVA followed by Dunnett test for multiple comparisons.
775
776 **Figure 5: Micrometastases experience high levels of stress and increase selenocysteine biosynthesis.**

777

778 (A) Levels of reactive oxygen species (ROS) in subcutaneous tumors vs micro and macrometastatic nodules from
779 NSG mice transplanted with two different patient melanomas, M481 and M405, measured by flow cytometry
780 with fluorescent dyes. CellROX DeepRed was used to measure cytoplasmic oxidative stress and CellROX Green
781 was used to measure mitochondrial oxidative stress levels. n = number of mice analyzed and indicated in the
782 figure. Mean +/- SD. Statistical significance assessed by one-way analysis of variance (ANOVAs) followed by
783 Dunnett's tests for multiple comparisons.

784 (B) Transcript levels of selenocysteine biosynthesis machinery in subcutaneous tumors vs micro and
785 macrometastatic nodules from NSG mice transplanted with patient-derived melanoma, M481, measured by qRT-
786 PCR. Mean +/- SD of 3 independent replicates; One-way analysis of variance (ANOVAs) followed by Dunnett's
787 tests for multiple comparisons.

788 (C) Levels of selenoproteins, FTSJ1 and WDR6 in metastases compared to primary tumor tissues from NSG mice
789 transplanted with patient-derived melanoma, M405, measured by immunofluorescent staining. Representative
790 shown from 3 independent experiments.

791 (D) Levels of selenoproteins and components of selenocysteine biosynthesis machinery in metastases compared to
792 primary tumor from NSG mice transplanted with patient-derived melanomas, M405 and M481, as measured by
793 western blotting. Representative shown from 3 independent experiments.

794 (E) Levels of FTSJ1 in subcutaneous vs micro vs macrometastatic nodules from NSG mice transplanted with Mewo
795 melanoma cell lines, measured by immunofluorescence.

796 (F) Quantification of data shown in (E). n= number of tumors analyzed and indicated in the figure. Mean +/- SD. Two-
797 tailed one sample t-test.

798 (G) Levels of Um34 modification in subcutaneous tumors vs metastatic nodules from NSG mice transplanted with
799 two different patient-derived melanomas, M405 and M481, measured by LC-MS/MS analysis of modified $tRNA^{Sec}$
800 nucleosides. n= number of mice per melanoma indicated in the figure. Mean +/- SD. One-way analysis of variance
801 (ANOVA) (Kruskal-Wallis test) followed by Dunn's test for multiple comparisons.

802

803 **Figure 6: $tRNA^{Sec}$ Um34 modification is necessary and sufficient for metastasis *in vivo***

804 (A) Subcutaneous tumor growth in mice transplanted with either Control or *FTSJ1*-KO A375 melanoma cells. Data reflect
805 3 independent experiments but only one representative experiment is shown. Mean +/- SD. For each experiment n= 5
806 mice.
807 (B) Total metastatic burden in the visceral organs of mice subcutaneously transplanted with either Control or *FTSJ1*-KO
808 A375 melanoma cells. n= number of mice analyzed, indicated in the figure. Mean +/- SD. Two-tailed Mann-Whitney t-test.
809 (C) Subcutaneous tumor growth in mice transplanted with either Control or *FTSJ1* KD MeWo melanoma cells. Data reflect
810 3 independent experiments but only one representative experiment is shown. For each experiment n= 5 mice.
811 Mean +/- SD.
812 (D) Total metastatic burden in the visceral organs of mice subcutaneously transplanted with either Control of *FTSJ1* KD
813 MeWo melanoma cells. n = number of mice analyzed, indicated in the figure. Mean +/- SD. One-way analysis of variance
814 (ANOVA) followed by unpaired t with Welch's correction (two-tailed).
815 (E, G) Growth of subcutaneous tumors in mice transplanted with patient-derived melanoma, M405 (E) or M481 (G),
816 expressing either control or *FTSJ1*-targeting shRNAs. For each experiment n= 5 mice. Mean +/- SD.
817 (F, H) Total metastatic burden in visceral organs of mice transplanted with a patient-derived melanoma, M405 (F), or
818 M481 (H) expressing either control or *FTSJ1*-targeting shRNAs. n = number of mice analyzed, indicated in the figure. Mean
819 +/- SD. One-way analysis of variance (ANOVA) followed by unpaired t with Welch's correction (two-tailed).
820 (I) Subcutaneous tumor growth in mice transplanted with either Control or FTSJ1 overexpressing A375 melanoma cells.
821 Data reflect 3 independent experiments but only on representative experiment is shown. For each experiment n= 5 mice.
822 Mean +/- SD.
823 (J) Total metastatic burden in the visceral organs of mice subcutaneously transplanted with either Control or FTSJ1
824 overexpressing A375 melanoma cells. n = number of mice analyzed, indicated in the figure. Mean +/- SD. Two-tailed Mann-
825 Whitney t-test.
826 (K) Growth of subcutaneous tumors in mice transplanted from patient-derived melanoma, M481, overexpressing either
827 Renilla luciferase or FTSJ1. Data reflect 3 independent experiments but only on representative experiment is shown. For
828 each experiment n= 5 mice. Mean +/- SD.

829 (L) Total metastatic burden in visceral organs of mice transplanted with patient-derived melanoma, M481, overexpressing
830 either Renilla luciferase or FTSJ1. n = number of mice analyzed, indicated in the figure. Mean +/- SD. Two-tailed Mann-
831 Whitney t-test.

832

833

834

835

836 **REFERENCES**

837 1. Chan, C., Pham, P., Dedon, P.C. & Begley, T.J. Lifestyle modifications: coordinating the tRNA
838 epitranscriptome with codon bias to adapt translation during stress responses. *Genome Biol* **19**,
839 228 (2018).
840 2. Suzuki, T. The expanding world of tRNA modifications and their disease relevance. *Nat Rev Mol*
841 *Cell Biol* **22**, 375-392 (2021).
842 3. Agris, P.F., Narendran, A., Sarachan, K., Vare, V.Y.P. & Eruysal, E. The Importance of Being
843 Modified: The Role of RNA Modifications in Translational Fidelity. *Enzymes* **41**, 1-50 (2017).
844 4. Endres, L., Dedon, P.C. & Begley, T.J. Codon-biased translation can be regulated by wobble-base
845 tRNA modification systems during cellular stress responses. *RNA Biol* **12**, 603-614 (2015).
846 5. Hatfield, D.L., Tsuji, P.A., Carlson, B.A. & Gladyshev, V.N. Selenium and selenocysteine: roles in
847 cancer, health, and development. *Trends Biochem Sci* **39**, 112-120 (2014).
848 6. Fradejas-Villar, N. *et al.* The RNA-binding protein Secisbp2 differentially modulates UGA codon
849 reassignment and RNA decay. *Nucleic Acids Res* **45**, 4094-4107 (2017).
850 7. Small-Howard, A. *et al.* Supramolecular complexes mediate selenocysteine incorporation in vivo.
851 *Mol Cell Biol* **26**, 2337-2346 (2006).
852 8. Xu, X.M. *et al.* Evidence for direct roles of two additional factors, SECp43 and soluble liver antigen,
853 in the selenoprotein synthesis machinery. *J Biol Chem* **280**, 41568-41575 (2005).
854 9. Hatfield, D.L., Carlson, B.A., Xu, X.M., Mix, H. & Gladyshev, V.N. Selenocysteine incorporation
855 machinery and the role of selenoproteins in development and health. *Prog Nucleic Acid Res Mol*
856 *Biol* **81**, 97-142 (2006).
857 10. Kim, L.K. *et al.* Methylation of the ribosyl moiety at position 34 of selenocysteine tRNA[Ser]Sec is
858 governed by both primary and tertiary structure. *RNA* **6**, 1306-1315 (2000).
859 11. van den Born, E. *et al.* ALKBH8-mediated formation of a novel diastereomeric pair of wobble
860 nucleosides in mammalian tRNA. *Nat Commun* **2**, 172 (2011).
861 12. Songe-Moller, L. *et al.* Mammalian ALKBH8 possesses tRNA methyltransferase activity required
862 for the biogenesis of multiple wobble uridine modifications implicated in translational decoding.
863 *Mol Cell Biol* **30**, 1814-1827 (2010).
864 13. Diamond, A.M. *et al.* Dietary selenium affects methylation of the wobble nucleoside in the
865 anticodon of selenocysteine tRNA([Ser]Sec). *J Biol Chem* **268**, 14215-14223 (1993).

866 14. Howard, M.T., Carlson, B.A., Anderson, C.B. & Hatfield, D.L. Translational redefinition of UGA
867 codons is regulated by selenium availability. *J Biol Chem* **288**, 19401-19413 (2013).
868 15. Carlson, B.A. *et al.* Selective restoration of the selenoprotein population in a mouse hepatocyte
869 selenoproteinless background with different mutant selenocysteine tRNAs lacking Um34. *J Biol*
870 *Chem* **282**, 32591-32602 (2007).
871 16. Li, Z. *et al.* Ribosome stalling during selenoprotein translation exposes a ferroptosis vulnerability.
872 *Nat Chem Biol* **18**, 751-761 (2022).
873 17. Yant, L.J. *et al.* The selenoprotein GPX4 is essential for mouse development and protects from
874 radiation and oxidative damage insults. *Free Radic Biol Med* **34**, 496-502 (2003).
875 18. Ingold, I. *et al.* Selenium Utilization by GPX4 Is Required to Prevent Hydroperoxide-Induced
876 Ferroptosis. *Cell* **172**, 409-422 e421 (2018).
877 19. Jakupoglu, C. *et al.* Cytoplasmic thioredoxin reductase is essential for embryogenesis but
878 dispensable for cardiac development. *Mol Cell Biol* **25**, 1980-1988 (2005).
879 20. Conrad, M. *et al.* Essential role for mitochondrial thioredoxin reductase in hematopoiesis, heart
880 development, and heart function. *Mol Cell Biol* **24**, 9414-9423 (2004).
881 21. Tarrago, L. *et al.* The selenoprotein methionine sulfoxide reductase B1 (MSRB1). *Free Radic Biol*
882 *Med* **191**, 228-240 (2022).
883 22. Cox, A.G. *et al.* Selenoprotein H is an essential regulator of redox homeostasis that cooperates
884 with p53 in development and tumorigenesis. *Proc Natl Acad Sci U S A* **113**, E5562-5571 (2016).
885 23. Sreelatha, A. *et al.* Protein AMPylation by an Evolutionarily Conserved Pseudokinase. *Cell* **175**,
886 809-821 e819 (2018).
887 24. Addinsall, A.B., Wright, C.R., Andrikopoulos, S., van der Poel, C. & Stupka, N. Emerging roles of
888 endoplasmic reticulum-resident selenoproteins in the regulation of cellular stress responses and
889 the implications for metabolic disease. *Biochem J* **475**, 1037-1057 (2018).
890 25. Kohrle, J. Thyroid hormone deiodinases--a selenoenzyme family acting as gate keepers to thyroid
891 hormone action. *Acta Med Austriaca* **23**, 17-30 (1996).
892 26. Shetty, S.P. & Copeland, P.R. The Selenium Transport Protein, Selenoprotein P, Requires Coding
893 Sequence Determinants to Promote Efficient Selenocysteine Incorporation. *J Mol Biol* **430**, 5217-
894 5232 (2018).
895 27. Reich, H.J. & Hondal, R.J. Why Nature Chose Selenium. *ACS Chem Biol* **11**, 821-841 (2016).
896 28. Brigelius-Flohe, R. & Flohe, L. Selenium and redox signaling. *Arch Biochem Biophys* **617**, 48-59
897 (2017).
898 29. Piskounova, E. *et al.* Oxidative stress inhibits distant metastasis by human melanoma cells. *Nature*
899 **527**, 186-191 (2015).
900 30. Endres, L. *et al.* Alkbh8 Regulates Selenocysteine-Protein Expression to Protect against Reactive
901 Oxygen Species Damage. *PLoS One* **10**, e0131335 (2015).
902 31. Touat-Hamici, Z., Legrain, Y., Bulteau, A.L. & Chavatte, L. Selective up-regulation of human
903 selenoproteins in response to oxidative stress. *J Biol Chem* **289**, 14750-14761 (2014).
904 32. Hall, S. *et al.* Cellular Effects of Pyocyanin, a Secreted Virulence Factor of Pseudomonas
905 aeruginosa. *Toxins (Basel)* **8** (2016).
906 33. Zhu, Z., Guo, R., Li, Y., Li, S. & Tu, P. Comparison of three analytical methods for superoxide
907 produced by activated immune cells. *J Pharmacol Toxicol Methods* **101**, 106637 (2020).
908 34. Mistry, H.D. *et al.* Differential expression and distribution of placental glutathione peroxidases 1,
909 3 and 4 in normal and preeclamptic pregnancy. *Placenta* **31**, 401-408 (2010).

910 35. Li, J. *et al.* Intellectual disability-associated gene ftsj1 is responsible for 2'-O-methylation of
911 specific tRNAs. *EMBO Rep* **21**, e50095 (2020).
912 36. Nagayoshi, Y. *et al.* Loss of Ftsj1 perturbs codon-specific translation efficiency in the brain and is
913 associated with X-linked intellectual disability. *Sci Adv* **7** (2021).
914 37. Ingolia, N.T. Ribosome Footprint Profiling of Translation throughout the Genome. *Cell* **165**, 22-33
915 (2016).
916 38. McGlincy, N.J. & Ingolia, N.T. Transcriptome-wide measurement of translation by ribosome
917 profiling. *Methods* **126**, 112-129 (2017).
918 39. Karlenius, T.C. *et al.* The selenium content of cell culture serum influences redox-regulated gene
919 expression. *Biotechniques* **50**, 295-301 (2011).
920 40. Carlson, B.A., Xu, X.M., Gladyshev, V.N. & Hatfield, D.L. Selective rescue of selenoprotein
921 expression in mice lacking a highly specialized methyl group in selenocysteine tRNA. *J Biol Chem*
922 **280**, 5542-5548 (2005).
923 41. Guo, L. *et al.* Selenocysteine-Specific Mass Spectrometry Reveals Tissue-Distinct
924 Selenoproteomes and Candidate Selenoproteins. *Cell Chem Biol* **25**, 1380-1388 e1384 (2018).
925 42. Bak, D.W., Gao, J., Wang, C. & Weerapana, E. A Quantitative Chemoproteomic Platform to
926 Monitor Selenocysteine Reactivity within a Complex Proteome. *Cell Chem Biol* **25**, 1157-1167
927 e1154 (2018).
928 43. Schoenmakers, E. *et al.* Mutation in human selenocysteine transfer RNA selectively disrupts
929 selenoprotein synthesis. *J Clin Invest* **126**, 992-996 (2016).
930 44. Vindry, C. *et al.* A homozygous mutation in the human selenocysteine tRNA gene impairs UGA
931 recoding activity and selenoproteome regulation by selenium. *Nucleic Acids Res* (2023).
932 45. Quintana, E. *et al.* Human melanoma metastasis in NSG mice correlates with clinical outcome in
933 patients. *Sci Transl Med* **4**, 159ra149 (2012).
934 46. Moustafa, M.E. *et al.* Selective inhibition of selenocysteine tRNA maturation and selenoprotein
935 synthesis in transgenic mice expressing isopentenyladenosine-deficient selenocysteine tRNA.
936 *Mol Cell Biol* **21**, 3840-3852 (2001).
937 47. Fradejas-Villar, N. *et al.* The Effect of tRNA([Ser]Sec) Isopentenylation on Selenoprotein
938 Expression. *Int J Mol Sci* **22** (2021).
939 48. Guy, M.P. *et al.* Defects in tRNA Anticodon Loop 2'-O-Methylation Are Implicated in
940 Nonsyndromic X-Linked Intellectual Disability due to Mutations in FTSJ1. *Hum Mutat* **36**, 1176-
941 1187 (2015).
942 49. Takano, K. *et al.* A loss-of-function mutation in the FTSJ1 gene causes nonsyndromic X-linked
943 mental retardation in a Japanese family. *Am J Med Genet B Neuropsychiatr Genet* **147B**, 479-484
944 (2008).
945 50. Goodarzi, H. *et al.* Modulated Expression of Specific tRNAs Drives Gene Expression and Cancer
946 Progression. *Cell* **165**, 1416-1427 (2016).
947 51. Crain, P.F. Preparation and enzymatic hydrolysis of DNA and RNA for mass spectrometry.
948 *Methods Enzymol* **193**, 782-790 (1990).
949 52. Corish, P. & Tyler-Smith, C. Attenuation of green fluorescent protein half-life in mammalian cells.
950 *Protein Eng* **12**, 1035-1040 (1999).
951 53. Bak, D.W., Gao, J., Wang, C. & Weerapana, E. A Quantitative Chemoproteomic Platform to
952 Monitor Selenocysteine Reactivity within a Complex Proteome. *Cell Chem Biol* (2018).

953 54. Quintana, E. *et al.* Phenotypic heterogeneity among tumorigenic melanoma cells from patients
954 that is reversible and not hierarchically organized. *Cancer Cell* **18**, 510-523 (2010).
955 55. Quintana, E. *et al.* Efficient tumour formation by single human melanoma cells. *Nature* **456**, 593-
956 598 (2008).
957
958
959
960
961
962
963
964

Figure 1

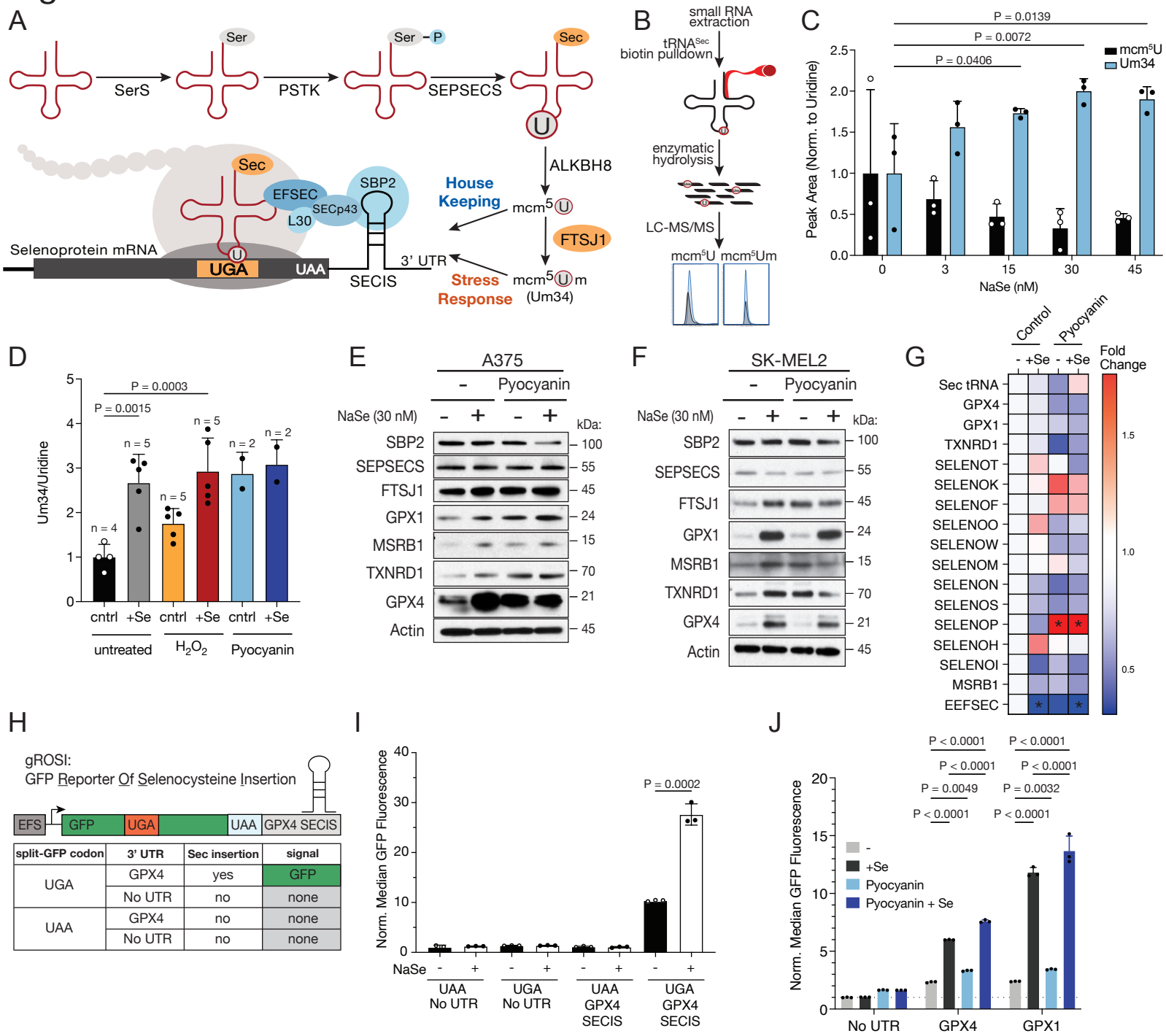
A
Ser
SerS
PSTK
Ser – P
SEPSECS
Sec
U
ALKBH8
Sec
EFSEC
SBP2
SECp43
L30
House Keeping
mcm5U
FTSJ1
Selenoprotein mRNA
UGA
UAA
3' UTR
SECIS
Stress Response
mcm5Um (Um34)
B
small RNA extraction
tRNASec biotin pulldown
enzymatic hydrolysis
LC-MS/MS
mcm5U mcm5Um
C
P = 0.0139
P = 0.0072
P = 0.0406
mcm5U
Um34
Peak Area (Norm. to Uridine)
NaSe (nM)
D
P = 0.0003
P = 0.0015
Um34/Uridine
n = 4
n = 5
n = 5
n = 5
n = 2
n = 2
cntrl
+Se
cntrl
+Se
cntrl
+Se
untreated
H2O2
Pyocyanin
E
A375
Pyocyanin
NaSe (30 nM)
kDa:
SBP2
SEPSECS
FTSJ1
GPX1
MSRB1
TXNRD1
GPX4
Actin
F
SK-MEL2
Pyocyanin
NaSe (30 nM)
kDa:
SBP2
SEPSECS
FTSJ1
GPX1
MSRB1
TXNRD1
GPX4
Actin
G
Control
Pyocyanin
Fold Change
Sec tRNA
GPX4
GPX1
TXNRD1
SELENOT
SELENOK
SELENOF
SELENOO
SELENOW
SELENOM
SELENON
SELENOS
SELENOP
SELENOH
SELENOI
MSRB1
EEFSEC
H
gROSI:
GFP Reporter Of Selenocysteine Insertion
EFS
GFP
UGA
UAA
GPX4 SECIS
split-GFP codon | 3' UTR | Sec insertion | signal
UGA | GPX4 | yes | GFP
UGA | No UTR | no | none
UAA | GPX4 | no | none
UAA | No UTR | no | none
I
Norm. Median GFP Fluorescence
P = 0.0002
NaSe
UAA No UTR
UGA No UTR
UAA GPX4 SECIS
UGA GPX4 SECIS
J
P < 0.0001
P < 0.0001
P = 0.0049
P < 0.0001
P < 0.0001
P < 0.0001
P = 0.0032
P < 0.0001
Norm. Median GFP Fluorescence
-
+Se
Pyocyanin
Pyocyanin + Se
No UTR
GPX4
GPX1

Figure 2

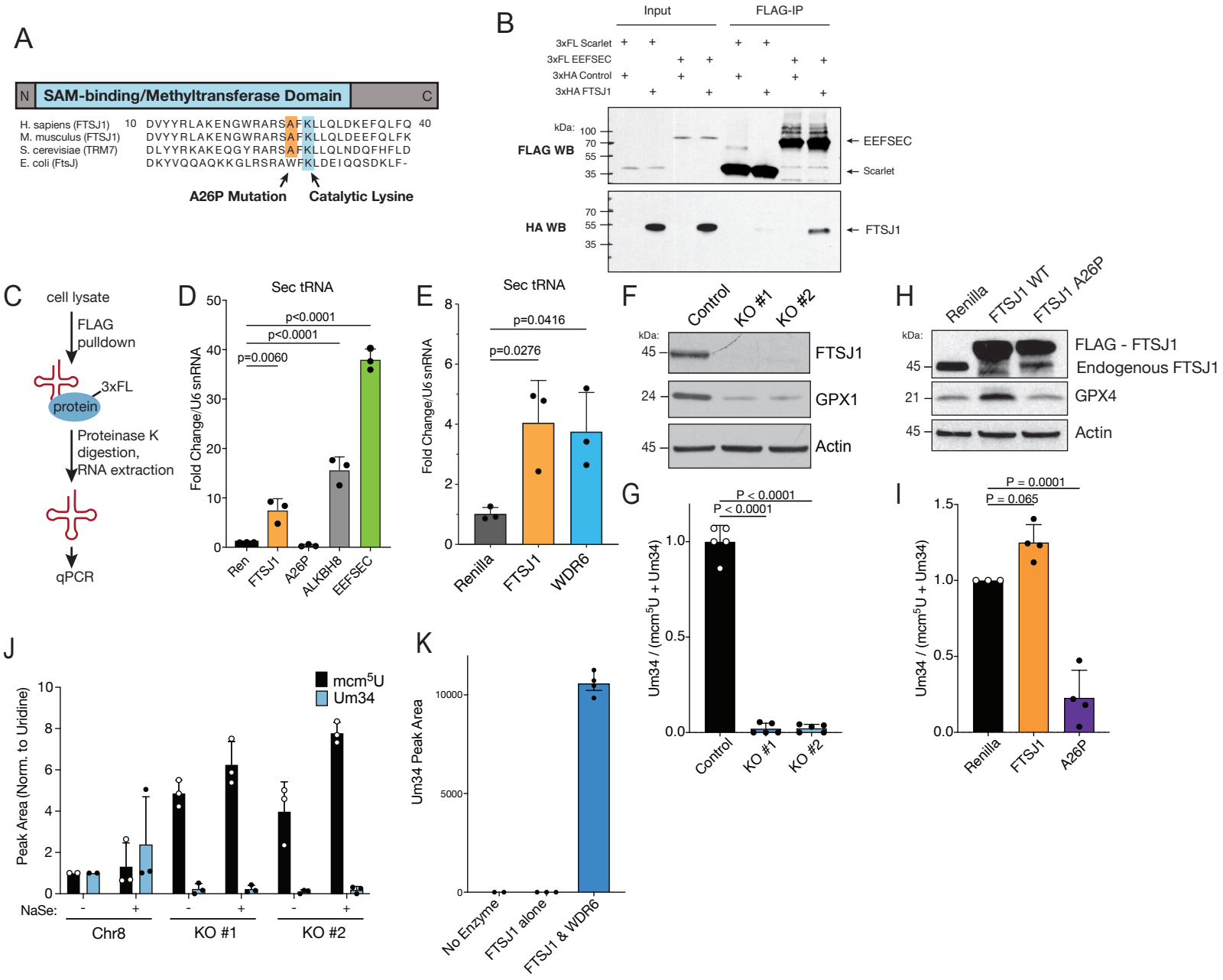
A
N
SAM-binding/Methyltransferase Domain
C
H. sapiens (FTSJ1) 10 DVYYRLAKENGWRARSAFKLLQLDKEFQLFQ 40
M. musculus (FTSJ1) DVYYRLAKENGWRARSAFKLLQLDEEFQLFK
S. cerevisiae (TRM7) DLYYRKAKEQGYRARSAFKLLQLNDQFHFLD
E. coli (FtsJ) DKYVQQAQKKGLRSRAWFKLDEIQQSDKLF-
A26P Mutation
Catalytic Lysine
B
Input
FLAG-IP
3xFL Scarlet
3xFL EEFSEC
3xHA Control
3xHA FTSJ1
kDa:
FLAG WB
HA WB
EEFSEC
Scarlet
FTSJ1
C
cell lysate
FLAG pulldown
3xFL
protein
Proteinase K digestion, RNA extraction
qPCR
D
Sec tRNA
Fold Change/U6 snRNA
p<0.0001
p<0.0001
p=0.0060
Ren
FTSJ1
A26P
ALKBH8
EEFSEC
E
Sec tRNA
Fold Change/U6 snRNA
p=0.0416
p=0.0276
Renilla
FTSJ1
WDR6
F
Control
KO #1
KO #2
kDa:
FTSJ1
GPX1
Actin
G
P < 0.0001
P < 0.0001
Um34 / (mcm5U + Um34)
Control
KO #1
KO #2
H
Renilla
FTSJ1 WT
FTSJ1 A26P
kDa:
FLAG - FTSJ1
Endogenous FTSJ1
GPX4
Actin
I
P = 0.0001
P = 0.065
Um34 / (mcm5U + Um34)
Renilla
FTSJ1
A26P
J
mcm5U
Um34
Peak Area (Norm. to Uridine)
NaSe:
Chr8
KO #1
KO #2
K
Um34 Peak Area
No Enzyme
FTSJ1 alone
FTSJ1 & WDR6

Figure 3

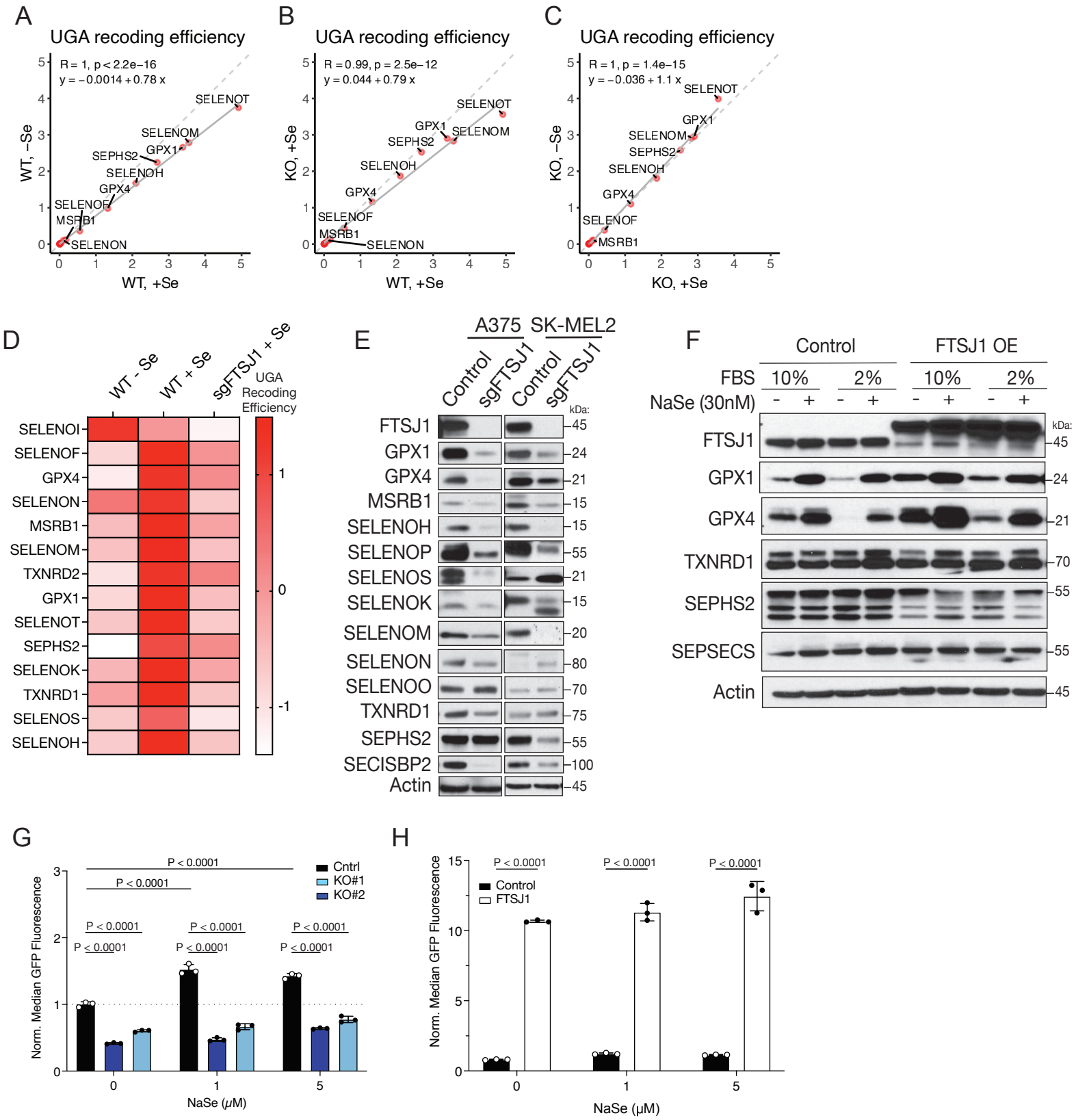
A
UGA recoding efficiency
R = 1, p < 2.2e−16
y = −0.0014 + 0.78 x
WT, −Se
WT, +Se
SELENOT
SELENOM
GPX1
SEPHS2
SELENOH
GPX4
SELENOF
MSRB1
SELENON
B
UGA recoding efficiency
R = 0.99, p = 2.5e−12
y = 0.044 + 0.79 x
KO, +Se
WT, +Se
C
UGA recoding efficiency
R = 1, p = 1.4e−15
y = −0.036 + 1.1 x
KO, −Se
KO, +Se
D
WT - Se
WT + Se
sgFTSJ1 + Se
UGA Recoding Efficiency
SELENOI
SELENOF
GPX4
SELENON
MSRB1
SELENOM
TXNRD2
GPX1
SELENOT
SEPHS2
SELENOK
TXNRD1
SELENOS
SELENOH
E
A375
SK-MEL2
Control
sgFTSJ1
Control
sgFTSJ1
kDa:
FTSJ1
GPX1
GPX4
MSRB1
SELENOH
SELENOP
SELENOS
SELENOK
SELENOM
SELENON
SELENOO
TXNRD1
SEPHS2
SECISBP2
Actin
F
Control
FTSJ1 OE
FBS
10%
2%
10%
2%
NaSe (30nM)
FTSJ1
GPX1
GPX4
TXNRD1
SEPHS2
SEPSECS
Actin
G
Norm. Median GFP Fluorescence
P < 0.0001
Cntrl
KO#1
KO#2
NaSe (μM)
H
Norm. Median GFP Fluorescence
P < 0.0001
Control
FTSJ1
NaSe (μM)

Figure 4

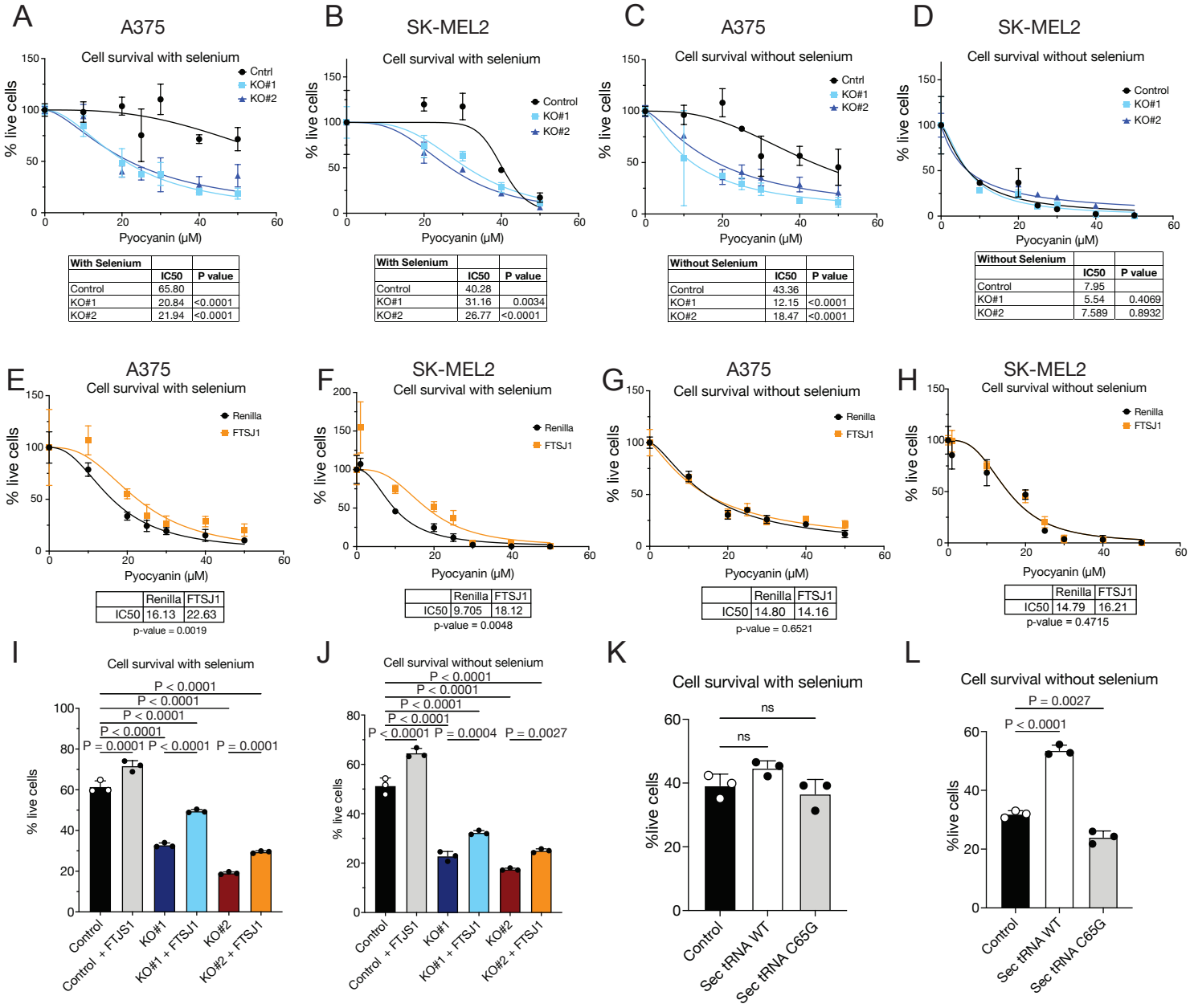

With Selenium		
	IC50	P value
Control	65.80	
KO#1	20.84	<0.0001
KO#2	21.94	<0.0001

With Selenium		
	IC50	P value
Control	40.28	
KO#1	31.16	0.0034
KO#2	26.77	<0.0001

Without Selenium		
	IC50	P value
Control	43.36	
KO#1	12.15	<0.0001
KO#2	18.47	<0.0001

Without Selenium		
	IC50	P value
Control	7.95	
KO#1	5.54	0.4069
KO#2	7.589	0.8932

	Renilla	FTSJ1
IC50	16.13	22.63

p-value = 0.0019

	Renilla	FTSJ1
IC50	9.705	18.12

p-value = 0.0048

	Renilla	FTSJ1
IC50	14.80	14.16

p-value = 0.6521

	Renilla	FTSJ1
IC50	14.79	16.21

p-value = 0.4715

Figure 5

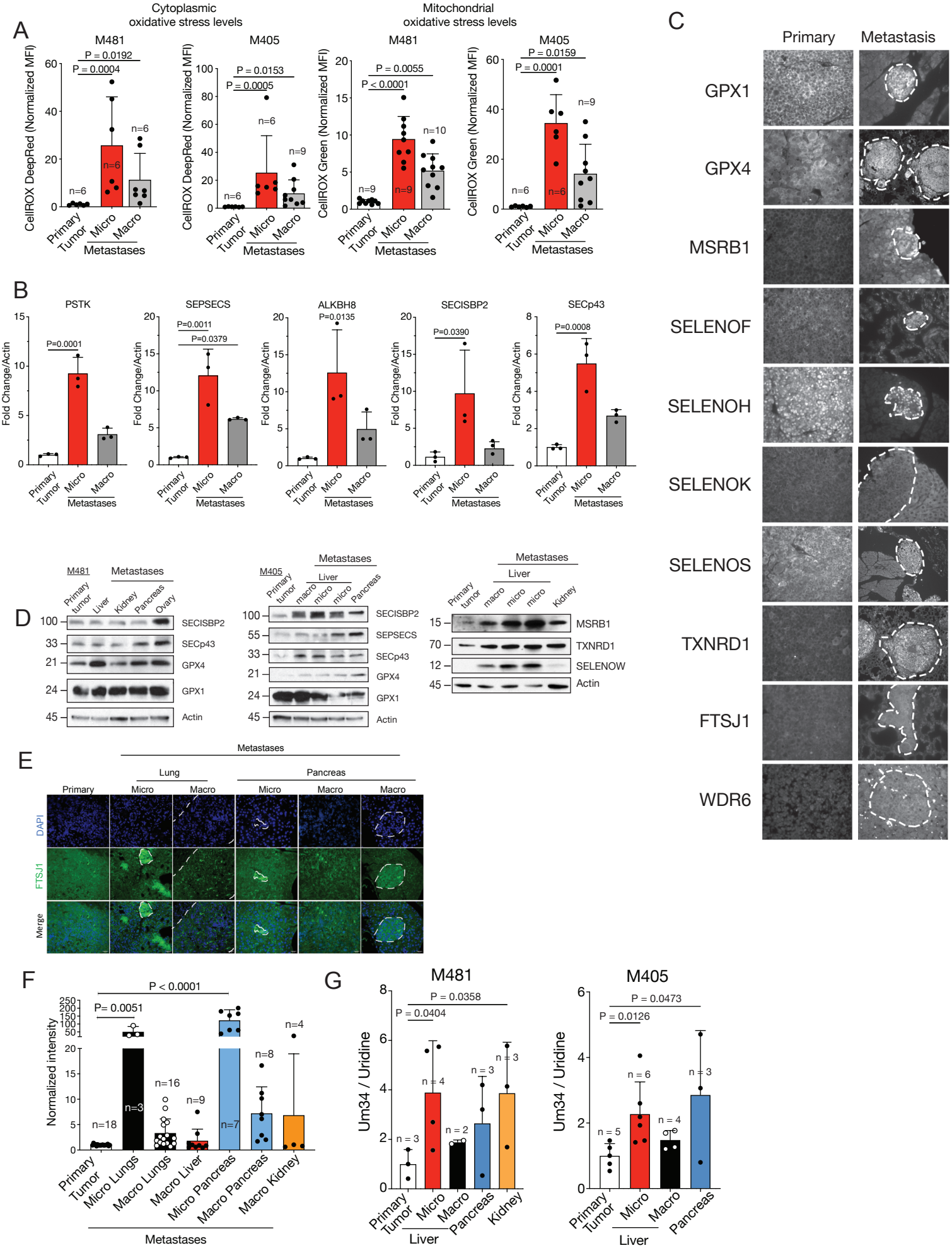
A
Cytoplasmic oxidative stress levels
Mitochondrial oxidative stress levels
M481
M405
CellROX DeepRed (Normalized MFI)
CellROX Green (Normalized MFI)
P = 0.0192
P = 0.0004
P = 0.0153
P = 0.0005
P = 0.0055
P < 0.0001
P = 0.0159
P = 0.0001
Primary Tumor
Micro
Macro
Metastases
B
PSTK
SEPSECS
ALKBH8
SECISBP2
SECp43
Fold Change/Actin
P=0.0001
P=0.0011
P=0.0379
P=0.0135
P=0.0390
P=0.0008
C
Primary
Metastasis
GPX1
GPX4
MSRB1
SELENOF
SELENOH
SELENOK
SELENOS
TXNRD1
FTSJ1
WDR6
D
M481
M405
Metastases
Liver
Primary tumor
Kidney
Pancreas
Ovary
macro
micro
SECISBP2
SECp43
GPX4
GPX1
Actin
SEPSECS
MSRB1
TXNRD1
SELENOW
E
Metastases
Lung
Pancreas
Primary
Micro
Macro
DAPI
FTSJ1
Merge
F
P < 0.0001
P= 0.0051
Normalized intensity
Primary Tumor
Micro Lungs
Macro Lungs
Macro Liver
Micro Pancreas
Macro Pancreas
Macro Kidney
G
M481
M405
P = 0.0358
P = 0.0404
P = 0.0473
P = 0.0126
Um34 / Uridine
Primary Tumor
Micro
Macro
Pancreas
Kidney
Liver

Figure 6

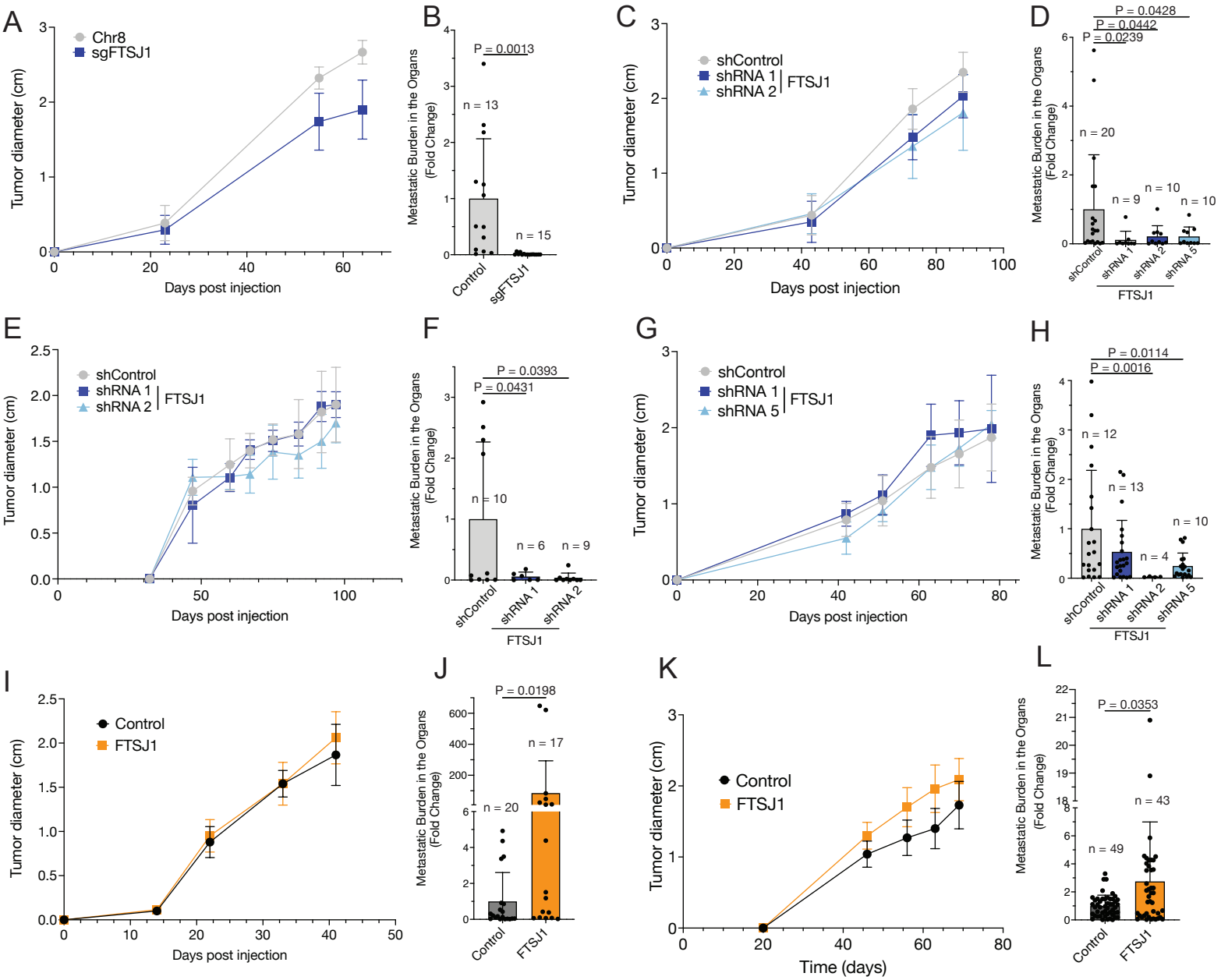
A
Chr8
sgFTSJ1
Tumor diameter (cm)
Days post injection
B
P = 0.0013
n = 13
n = 15
Metastatic Burden in the Organs (Fold Change)
Control
sgFTSJ1
C
shControl
shRNA 1
shRNA 2
FTSJ1
Tumor diameter (cm)
Days post injection
D
P = 0.0428
P = 0.0442
P = 0.0239
n = 20
n = 9
n = 10
n = 10
Metastatic Burden in the Organs (Fold Change)
shControl
shRNA 1
shRNA 2
shRNA 5
FTSJ1
E
shControl
shRNA 1
shRNA 2
FTSJ1
Tumor diameter (cm)
Days post injection
F
P = 0.0393
P = 0.0431
n = 10
n = 6
n = 9
Metastatic Burden in the Organs (Fold Change)
shControl
shRNA 1
shRNA 2
FTSJ1
G
shControl
shRNA 1
shRNA 5
FTSJ1
Tumor diameter (cm)
Days post injection
H
P = 0.0114
P = 0.0016
n = 12
n = 13
n = 4
n = 10
Metastatic Burden in the Organs (Fold Change)
shControl
shRNA 1
shRNA 2
shRNA 5
FTSJ1
I
Control
FTSJ1
Tumor diameter (cm)
Days post injection
J
P = 0.0198
n = 17
n = 20
Metastatic Burden in the Organs (Fold Change)
Control
FTSJ1
K
Control
FTSJ1
Tumor diameter (cm)
Time (days)
L
P = 0.0353
n = 43
n = 49
Metastatic Burden in the Organs (Fold Change)
Control
FTSJ1

Extended Figure 1

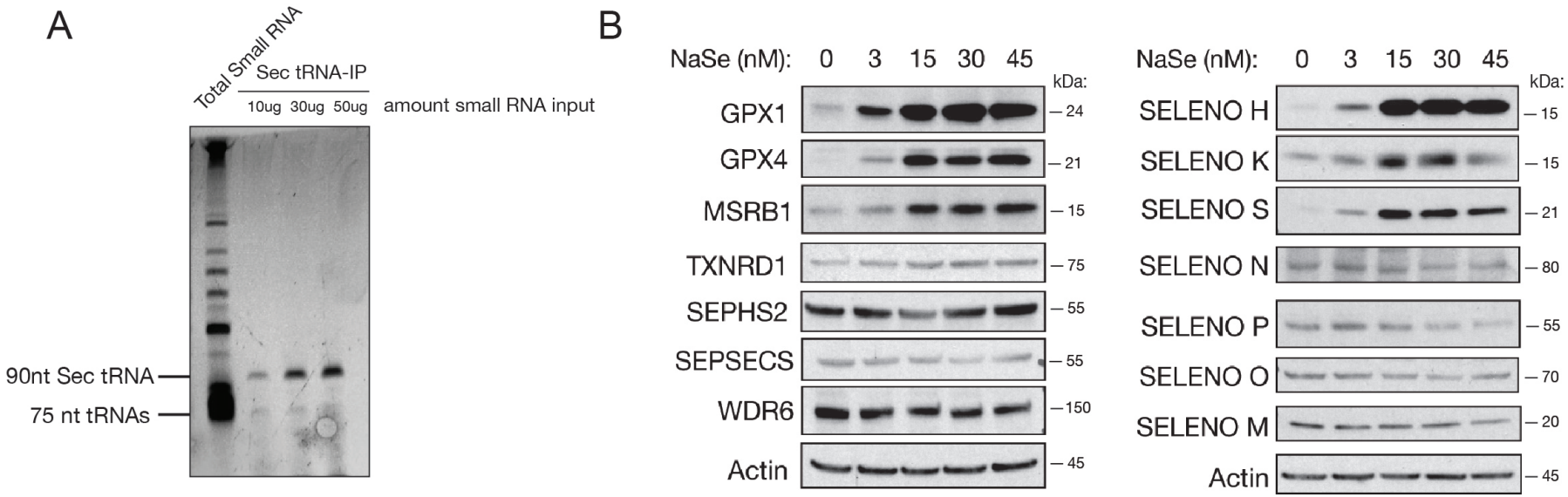

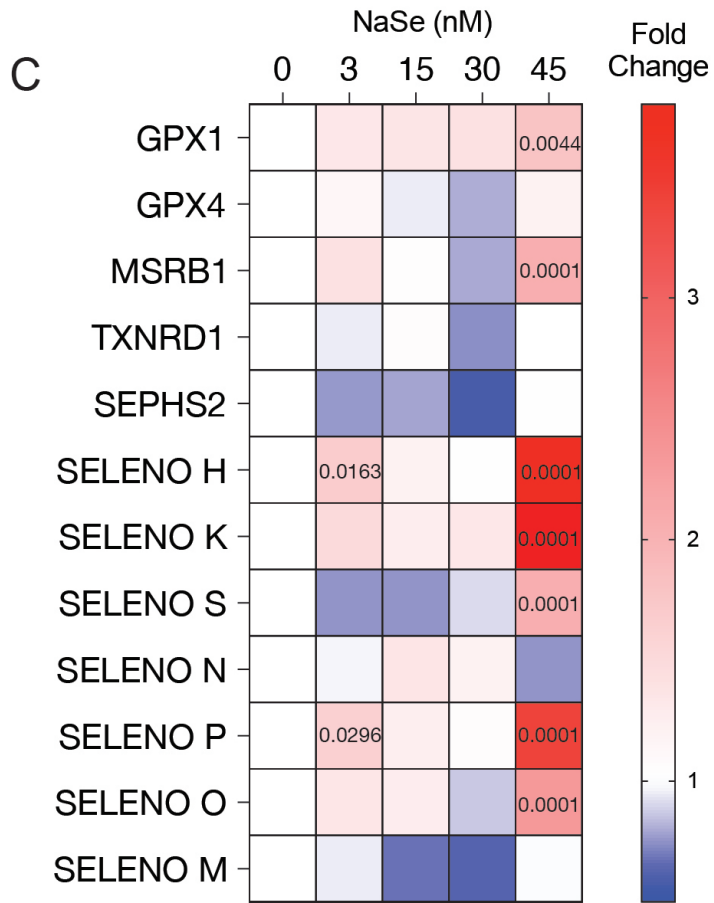

Extended Figure 2

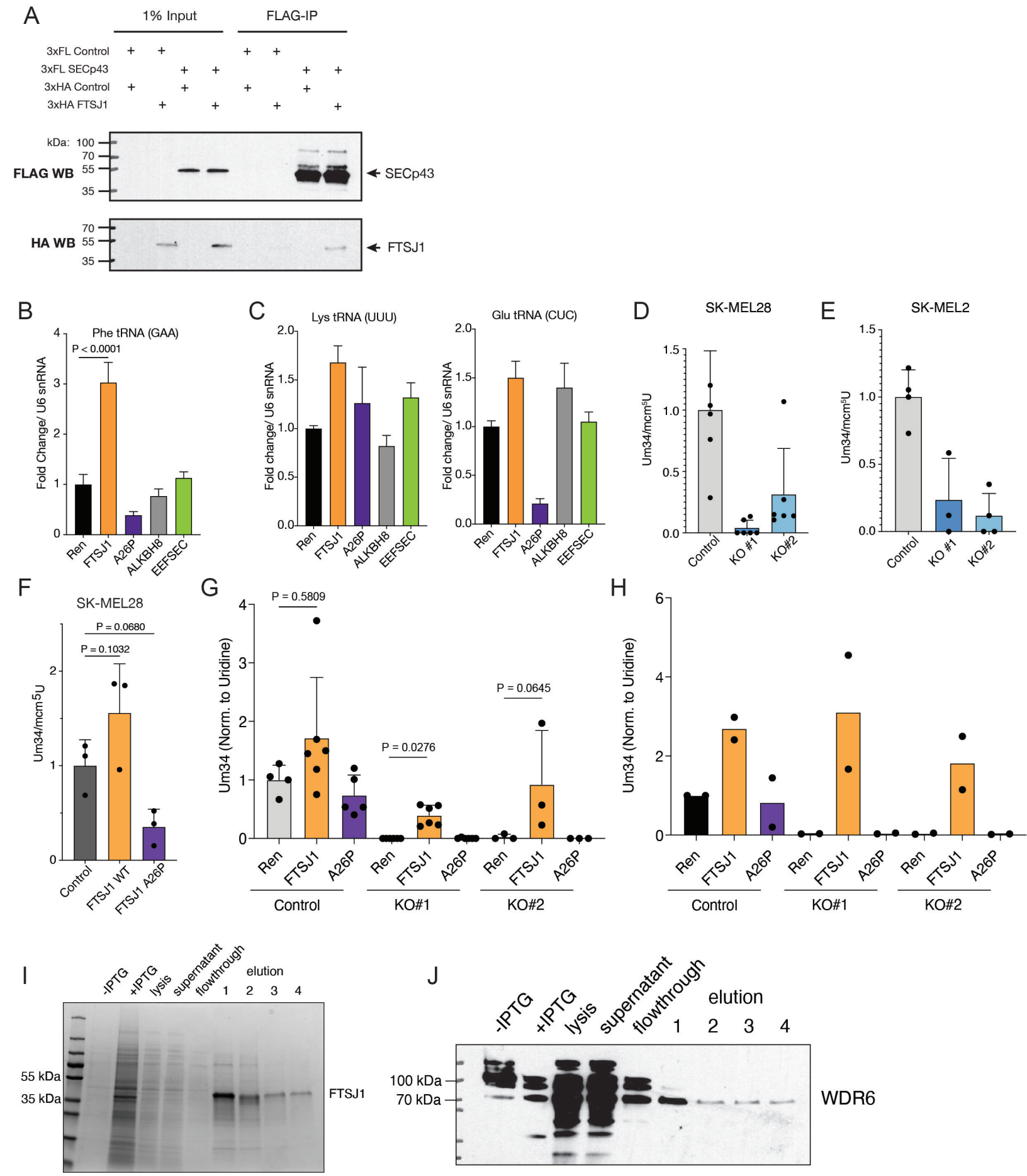

Extended Figure 5

A

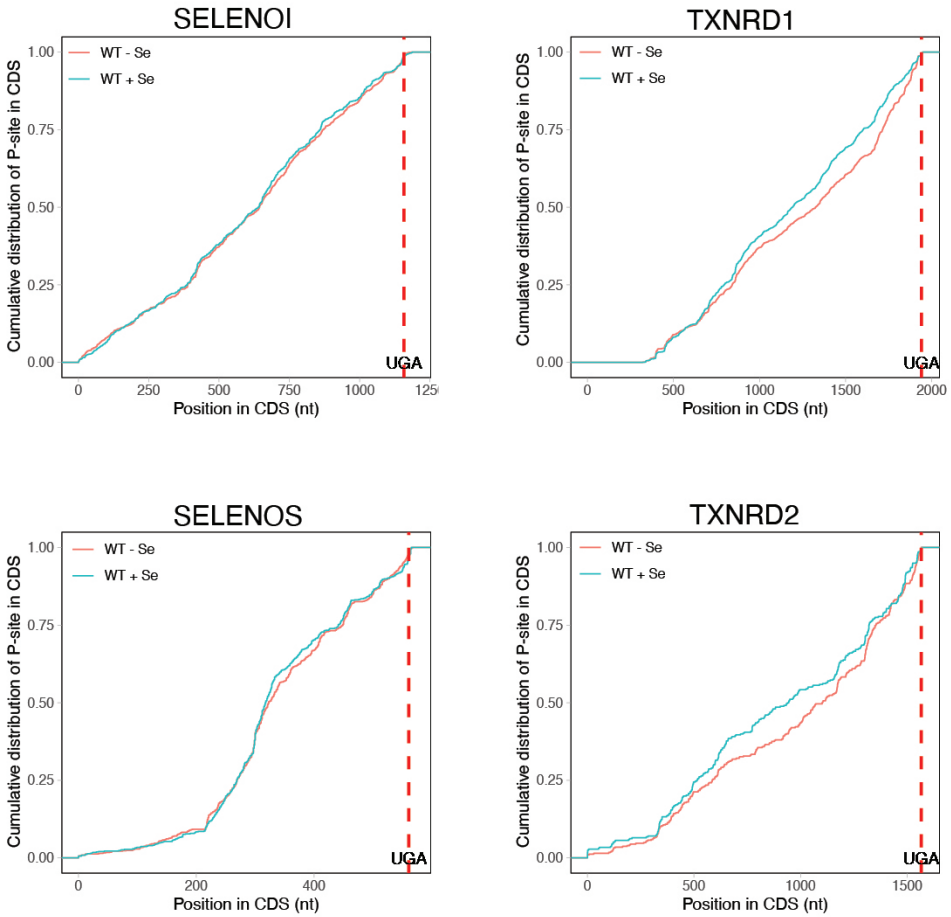

B

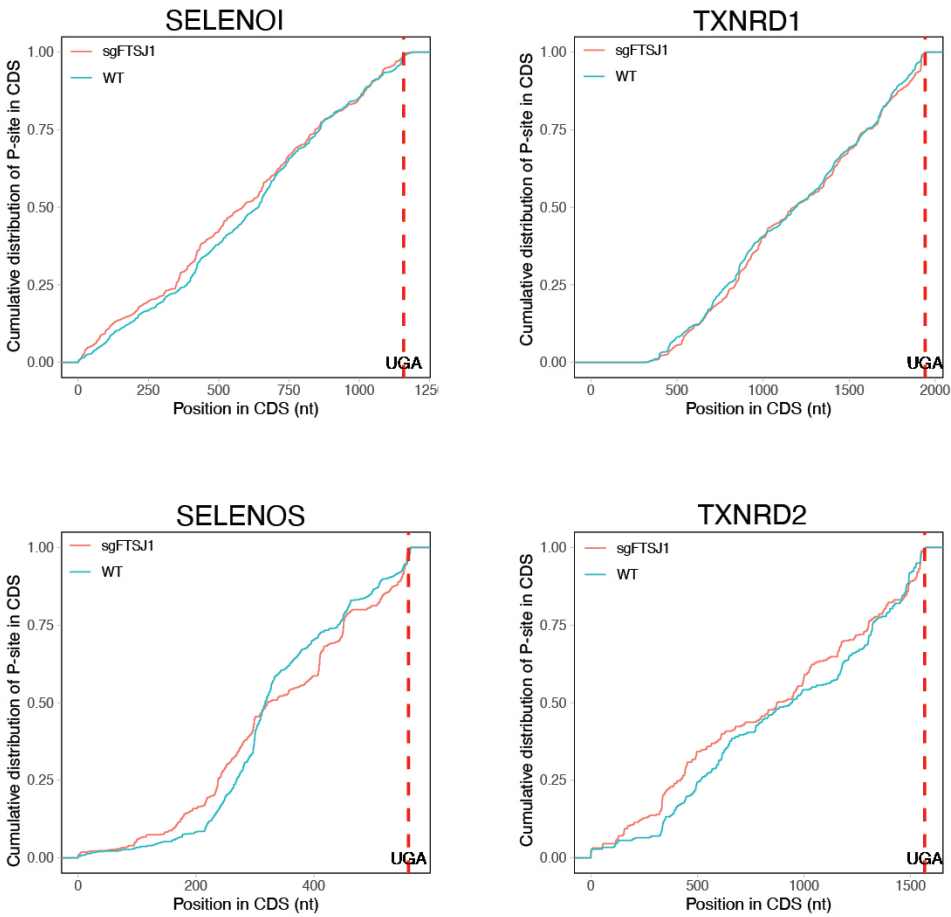

Extended Figure 4

A

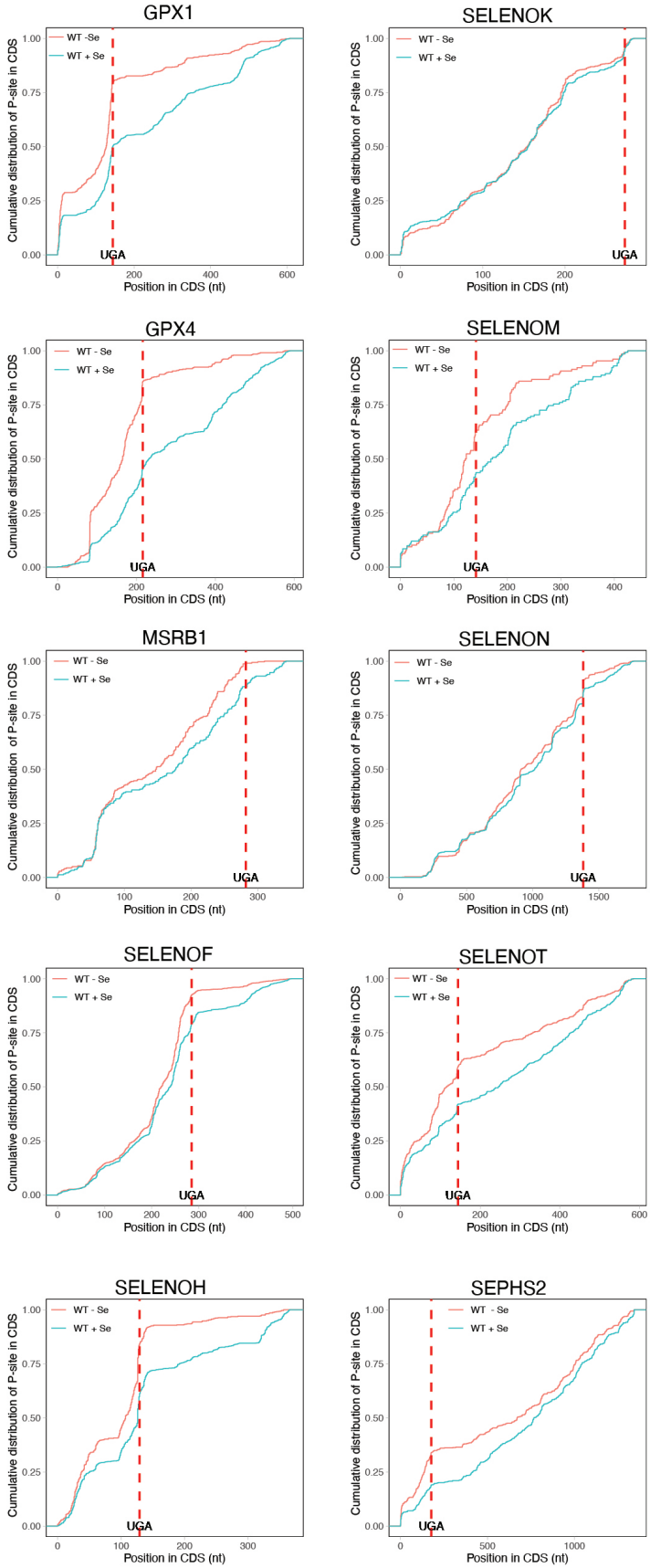

B

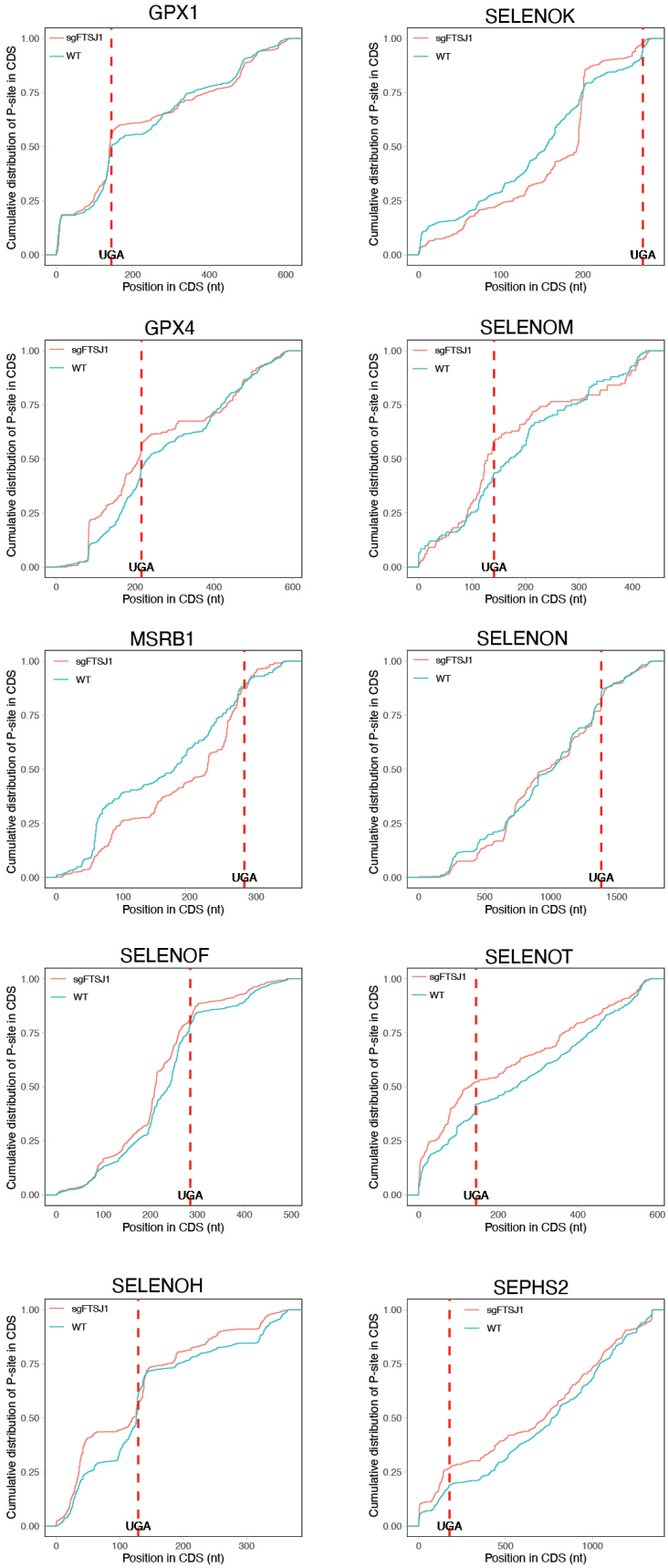

Extended Figure 3

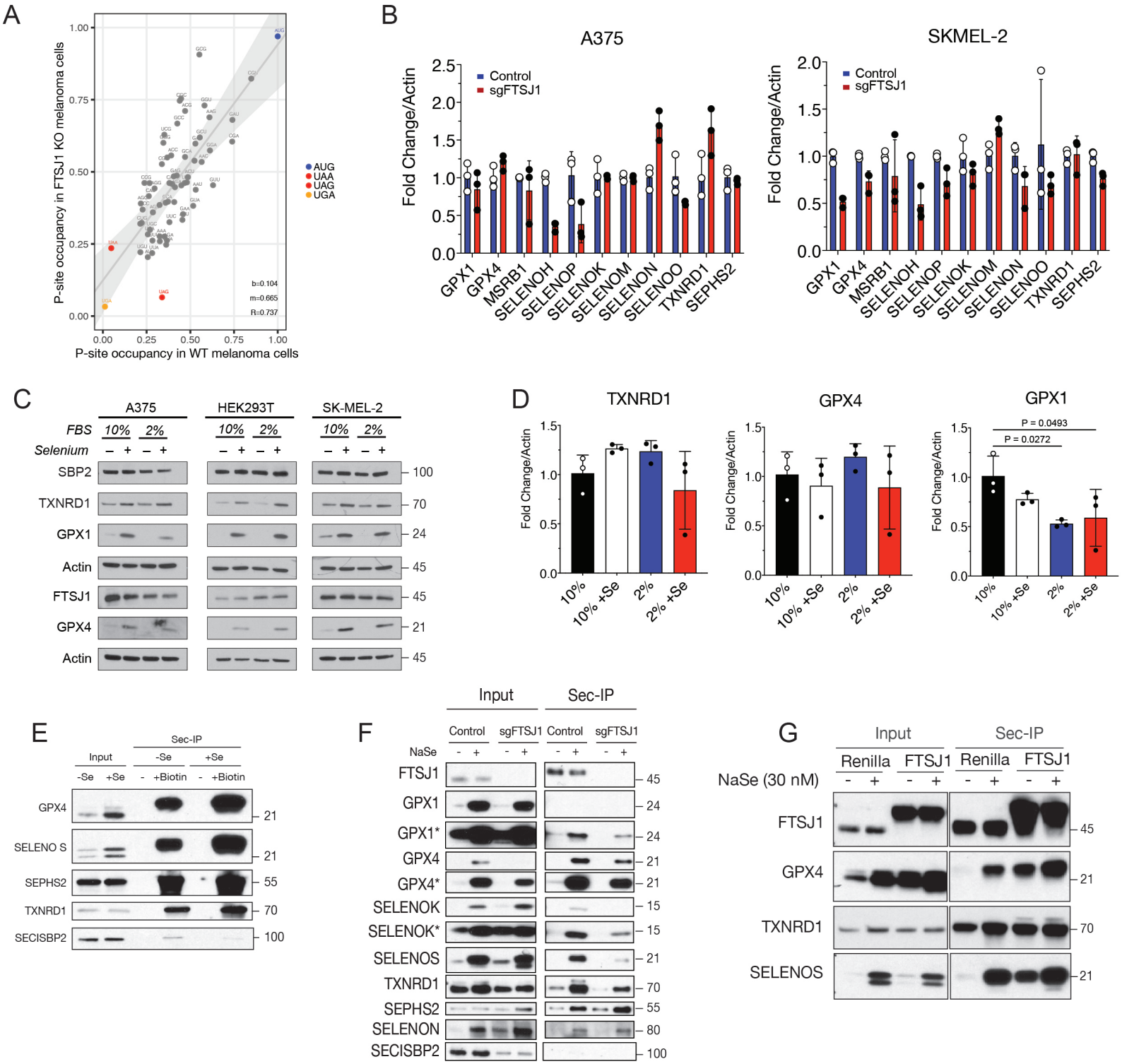

Extended Figure 6

Control sgFTSJ1

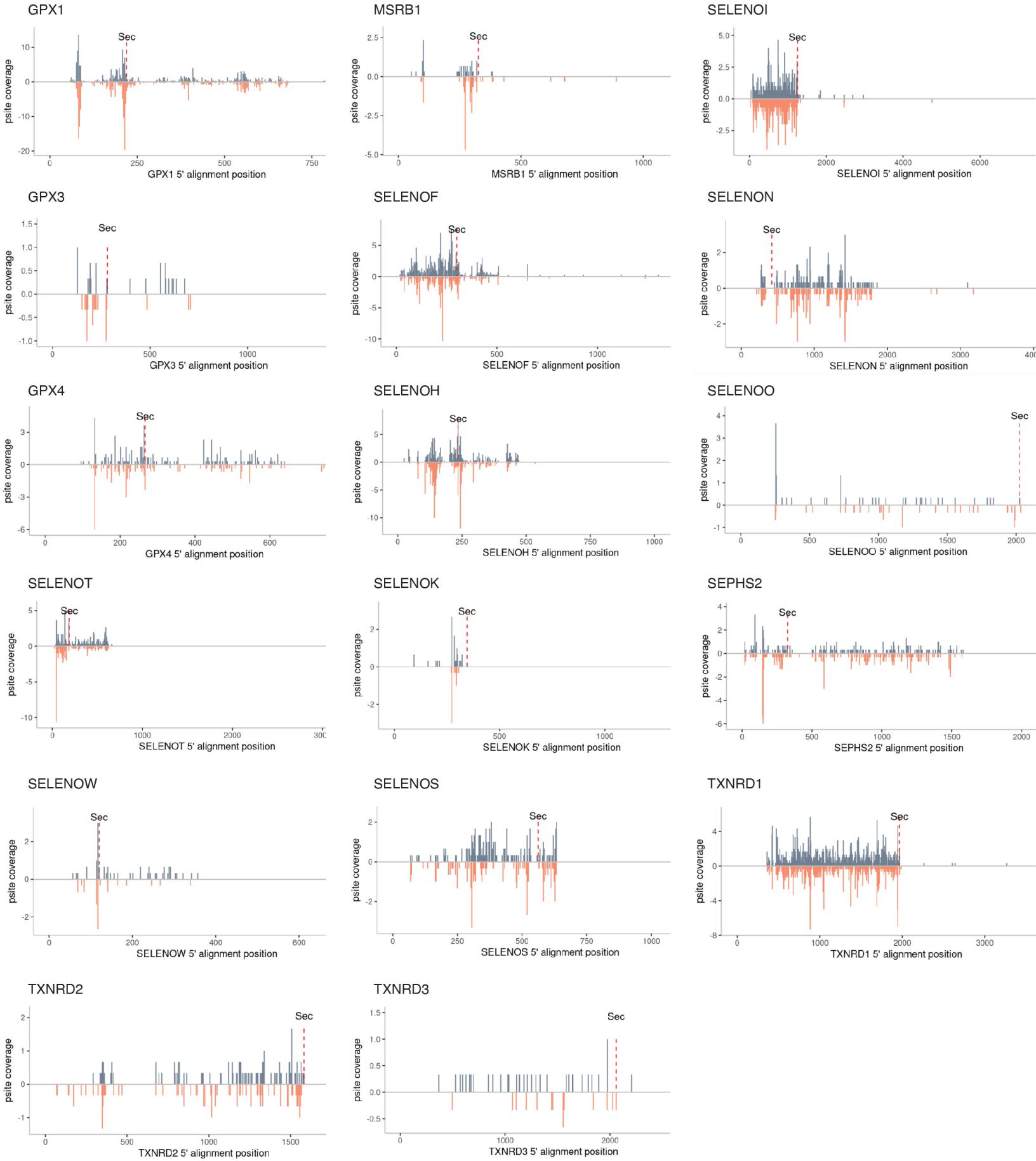

Extended Figure 7

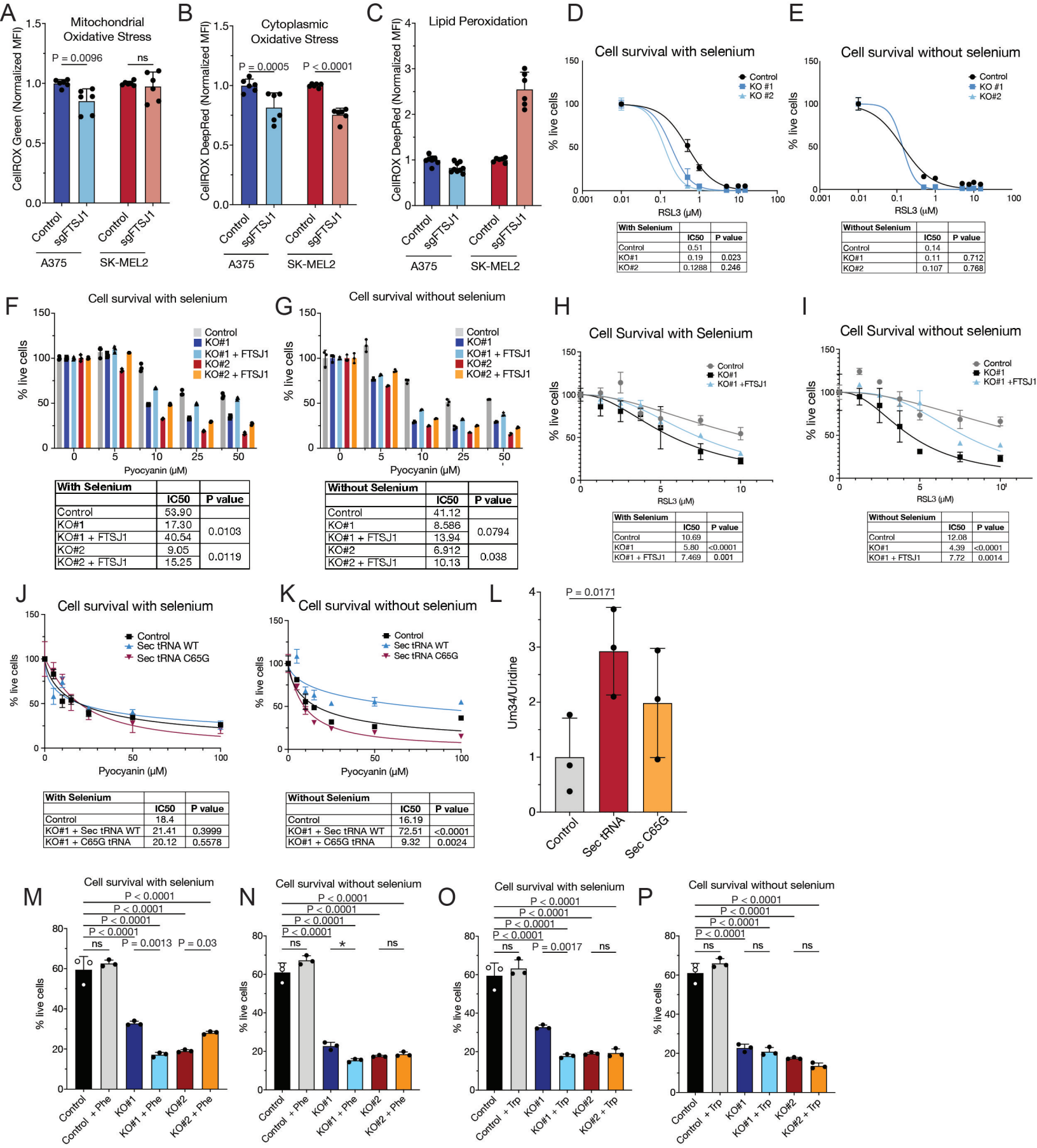

With Selenium	IC50	P value
Control	0.51	
KO#1	0.19	0.023
KO#2	0.1288	0.246

Without Selenium	IC50	P value
Control	0.14	
KO#1	0.11	0.712
KO#2	0.107	0.768

With Selenium	IC50	P value
Control	53.90	
KO#1	17.30	0.0103
KO#1 + FTSJ1	40.54	
KO#2	9.05	0.0119
KO#2 + FTSJ1	15.25	

Without Selenium	IC50	P value
Control	41.12	
KO#1	8.586	0.0794
KO#1 + FTSJ1	13.94	
KO#2	6.912	0.038
KO#2 + FTSJ1	10.13	

With Selenium	IC50	P value
Control	10.69	
KO#1	5.80	<0.0001
KO#1 + FTSJ1	7.469	0.001

Without Selenium	IC50	P value
Control	12.08	
KO#1	4.39	<0.0001
KO#1 + FTSJ1	7.72	0.0014

With Selenium	IC50	P value
Control	18.4	
KO#1 + Sec tRNA WT	21.41	0.3999
KO#1 + C65G tRNA	20.12	0.5578

Without Selenium	IC50	P value
Control	16.19	
KO#1 + Sec tRNA WT	72.51	<0.0001
KO#1 + C65G tRNA	9.32	0.0024

Extended Figure 8

A

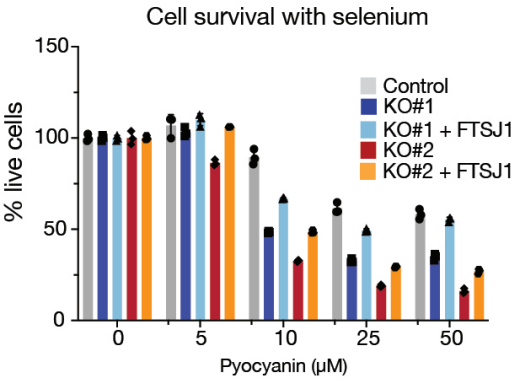

With Selenium		
	IC50	P value
Control	53.90	
KO#1	17.30	0.0103
KO#1 + FTSJ1	40.54	
KO#2	9.05	0.0119
KO#2 + FTSJ1	15.25	

B

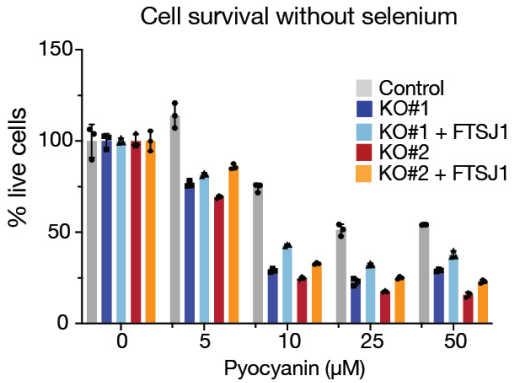

Without Selenium		
	IC50	P value
Control	41.12	
KO#1	8.586	0.0794
KO#1 + FTSJ1	13.94	
KO#2	6.912	0.038
KO#2 + FTSJ1	10.13	

C

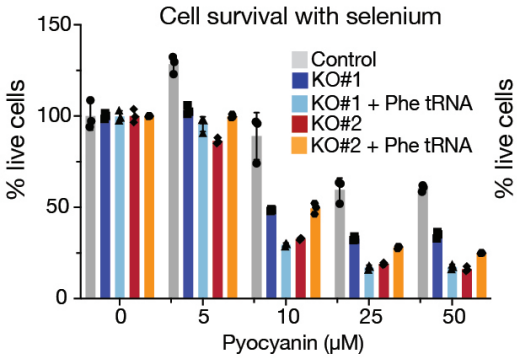

With Selenium		
	IC50	P value
Control	52.29	
KO#1	17.30	0.0012
KO#1 + Phe	8.51	
KO#2	9.05	0.0108
KO#2 + Phe	14.42	

D

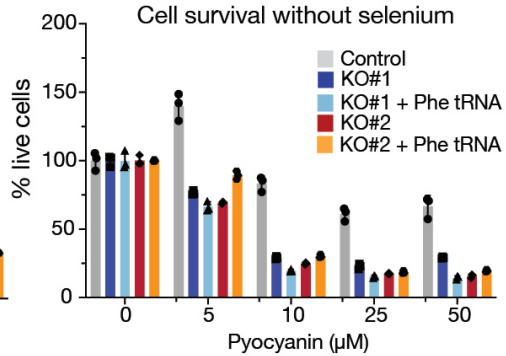

Without Selenium		
	IC50	P value
Control	62.65	
KO#1	8.59	0.1698
KO#1 + Phe	6.35	
KO#2	6.91	0.2023
KO#2 + Phe	8.29	

E

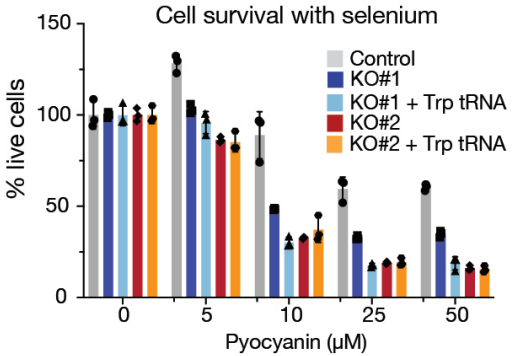

With Selenium		
	IC50	P value
Control	52.29	
KO#1	17.30	0.0025
KO#1 + Trp	8.57	
KO#2	9.05	0.6895
KO#2 + Trp	9.59	

F

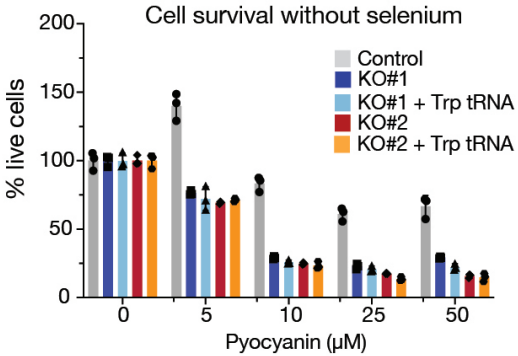

Without Selenium		
	IC50	P value
Control	62.65	
KO#1	8.59	0.5782
KO#1 + Trp	7.46	
KO#2	6.91	0.9906
KO#2 + Trp	6.90	

Extended Figure 9

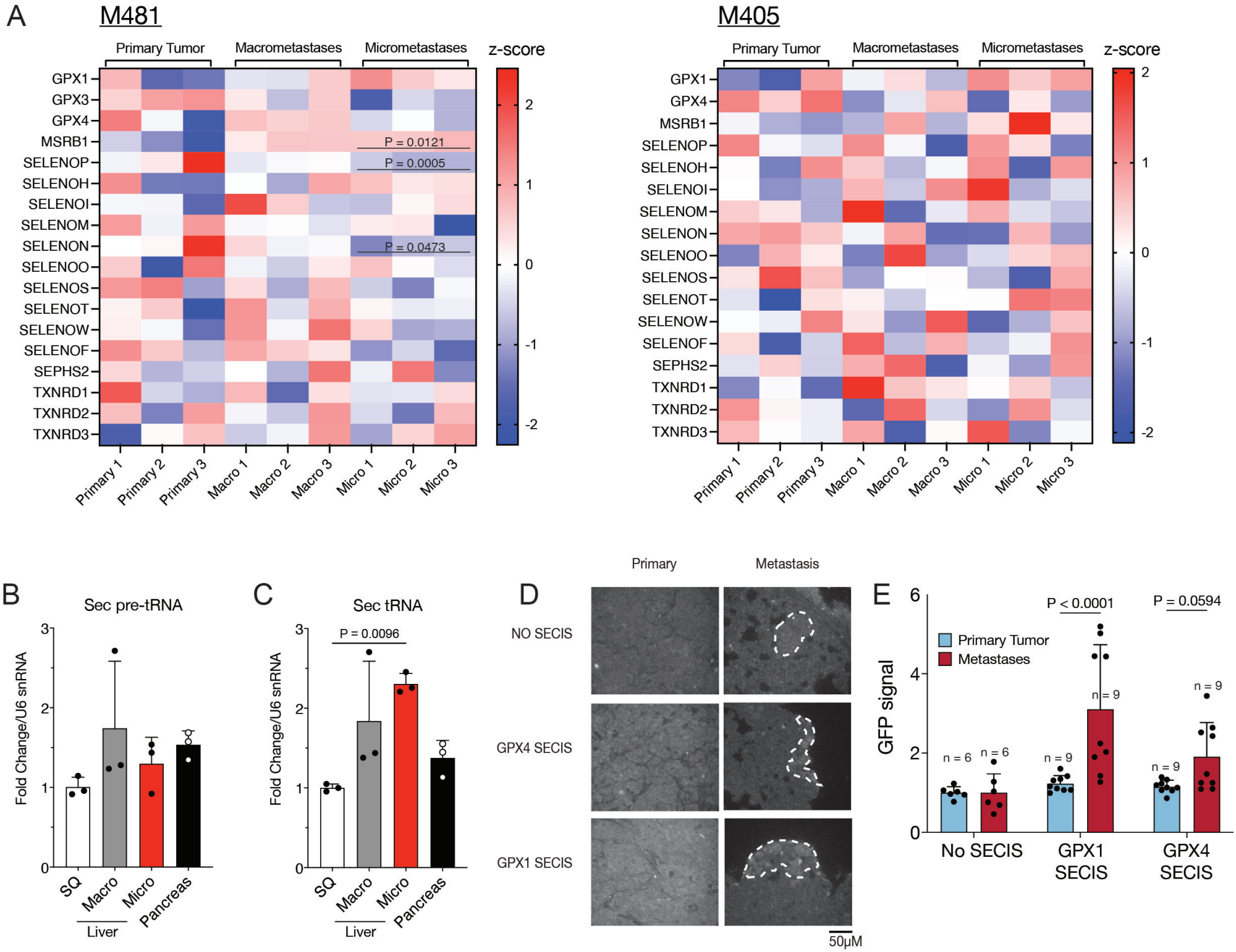
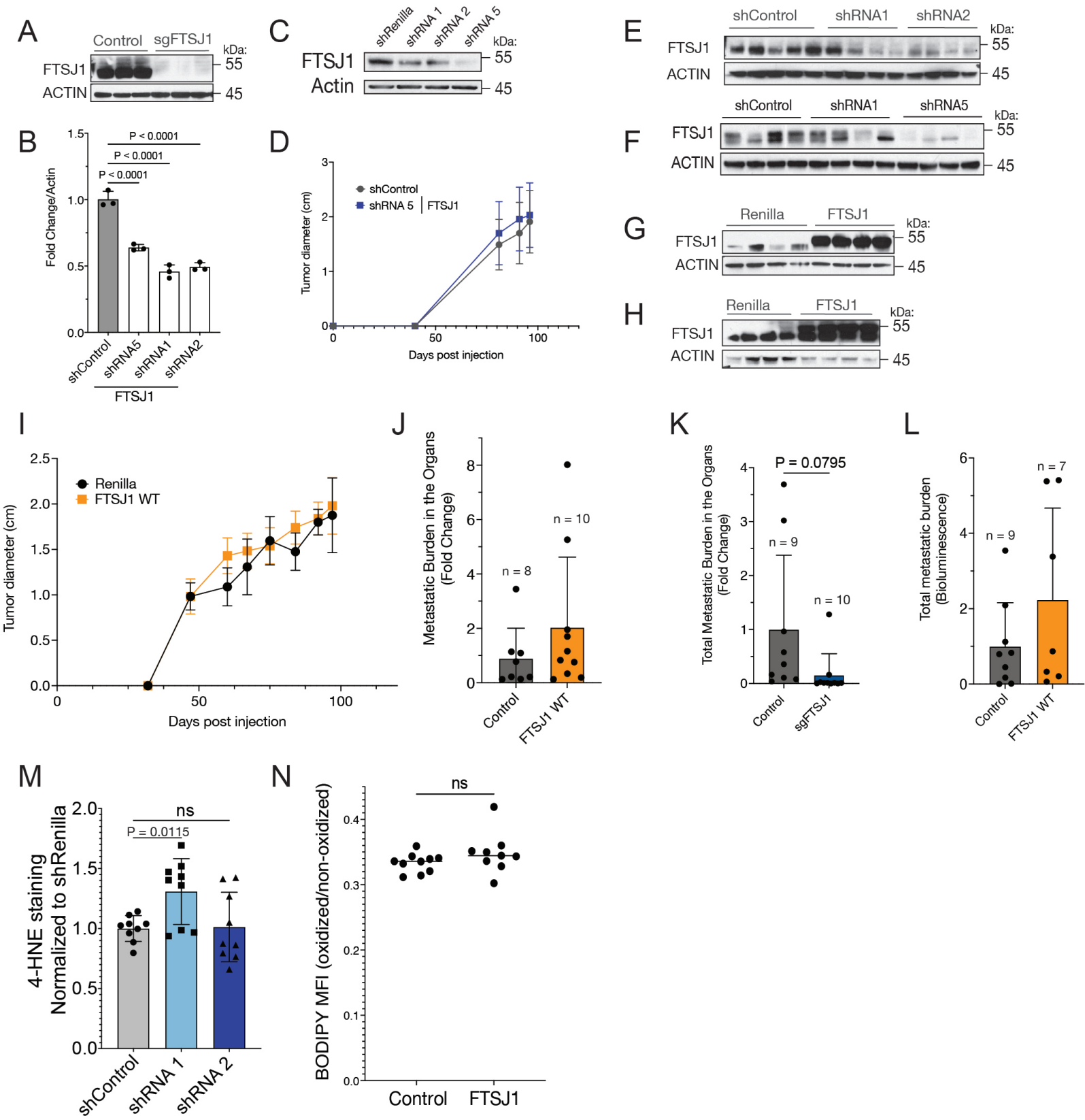
Extended Figure 10